Journal of Volcanology and Geothermal Research 329 (2017) 54–68

Contents lists available at ScienceDirect

Journal of Volcanology and Geothermal Research

journal homepage: www.elsevier.com/locate/jvolgeores

Oxygen isotope systematics in an evolving geothermal system: Coso Hot Springs, California

Thomas M. Etzel [a,b,*], John R. Bowman [a], Joseph N. Moore [b], John W. Valley [c], Michael J. Spicuzza [c], Jesse M. McCulloch [d]

[a] Dept. of Geology and Geophysics, University of Utah, Salt Lake City, UT 84112, USA
[b] Energy & Geoscience Institute, University of Utah, Salt Lake City, UT 84108, USA
[c] Dept. of Geoscience, University of Wisconsin, Madison, WI 54706, USA
[d] Terra-Gen Operating Company, Little Lake, CA, USA

ARTICLE INFO

Article history:
Received 22 July 2016
Received in revised form 22 November 2016
Accepted 22 November 2016
Available online 24 November 2016

ABSTRACT

Oxygen isotope and clay mineralogy studies have been made on whole rock samples and feldspar separates from three wells along the high temperature West Flank of the Coso geothermal system, California. The reservoir rocks have experienced variable $^{18}O/^{16}O$ depletion, with $\delta^{18}O$ values ranging from primary values of +7.5‰ down to −4.6‰. Spatial patterns of clay mineral distributions in the three wells are not closely correlated with the distributions expected from measured, pre-production temperature profiles, but do correlate with spatial patterns of $^{18}O/^{16}O$ depletion, indicating that the stability of clay minerals in the three wells is a function of fluid-rock interaction in addition to temperature. Detailed $\delta^{18}O$ measurements in the three wells identify a limited number of localized intervals of extensive $^{18}O/^{16}O$ depletion. These intervals document localized zones of higher permeability in the geothermal system that have experienced significant fluid infiltration, water-rock interaction and oxygen isotopic exchange with the geothermal fluids. The local zones of maximum $^{18}O/^{16}O$ depletion in each well correspond closely with current hot water production zones. Most feldspar separates have measured $\delta^{18}O$ values too high to have completely attained oxygen isotope exchange equilibrium with the reservoir fluid at pre-production temperatures. In general, the lower the $\delta^{18}O$ value of the feldspar, the closer the feldspar approaches exchange equilibrium with the geothermal fluid. This correlation suggests that fracture-induced increases in permeability increase both fluid infiltration and the surface area of the host rock exposed to geothermal fluid, promoting fluid-rock interaction and oxygen isotope exchange. The two most $^{18}O/^{16}O$-depleted feldspar samples have $\delta^{18}O$ values too low to be in exchange equilibrium with the pre-production reservoir fluid at pre-production temperatures. These discrepancies suggest that the reservoir fluid in the West Flank of the Coso geothermal system was hotter and/or had a lower $\delta^{18}O$ value (due to fluid-rock interaction at higher permeability) in the past.
© 2016 Elsevier B.V. All rights reserved.

1. Introduction

The Coso Hot Springs Geothermal Field is located in China Lake, California, 10 km east of the Sierra Nevada Mountains at the western boundary of the Basin and Range Province (Fig. 1). Coso Hot Springs is a world-class geothermal field; it is the third largest producing geothermal field in the United States, among the hottest, with a current installed power capacity of 273 MWe and temperatures as high as 350 °C at depths as shallow as ~1 km. It is also one of the most extensively drilled geothermal systems, with many of the >150 wells reaching depths of 2–3 km.

The level of power production at Coso Hot Springs implies significant permeability in the reservoir rocks, which consist dominantly of metamorphosed Mesozoic diorite and younger granodiorite and granite. Although epidote, chlorite, illite, quartz, and calcite, which are typical of high-temperature geothermal systems worldwide (Henley and Ellis, 1983), are widespread at Coso Hot Springs, these minerals show no clear correlation with measured temperature in boreholes (Bishop and Bird, 1987; Lutz et al., 1996; Lutz and Moore, 1997; Kovac et al., 2004; Kovac et al., 2005). In contrast, minerals typical of moderate temperature environments, such as wairakite and prehnite, are rarely observed in the reservoir rocks.

Oxygen isotope measurements provide an alternative means of mapping changes in the extent of fluid-rock interactions, independent of bulk mineralogy, and have been applied extensively in both active geothermal systems (e.g. Lambert and Epstein, 1980; Sturchio et al., 1990; Smith and Suemnicht, 1991; White and Peterson, 1991; Moore

* Corresponding author at: Dept. of Geological Sciences, Jackson School of Geosciences, University of Texas at Austin, Austin, TX 78712, USA.
E-mail address: thomas.etzel@utexas.edu (T.M. Etzel).

http://dx.doi.org/10.1016/j.jvolgeores.2016.11.014
0377-0273/© 2016 Elsevier B.V. All rights reserved.

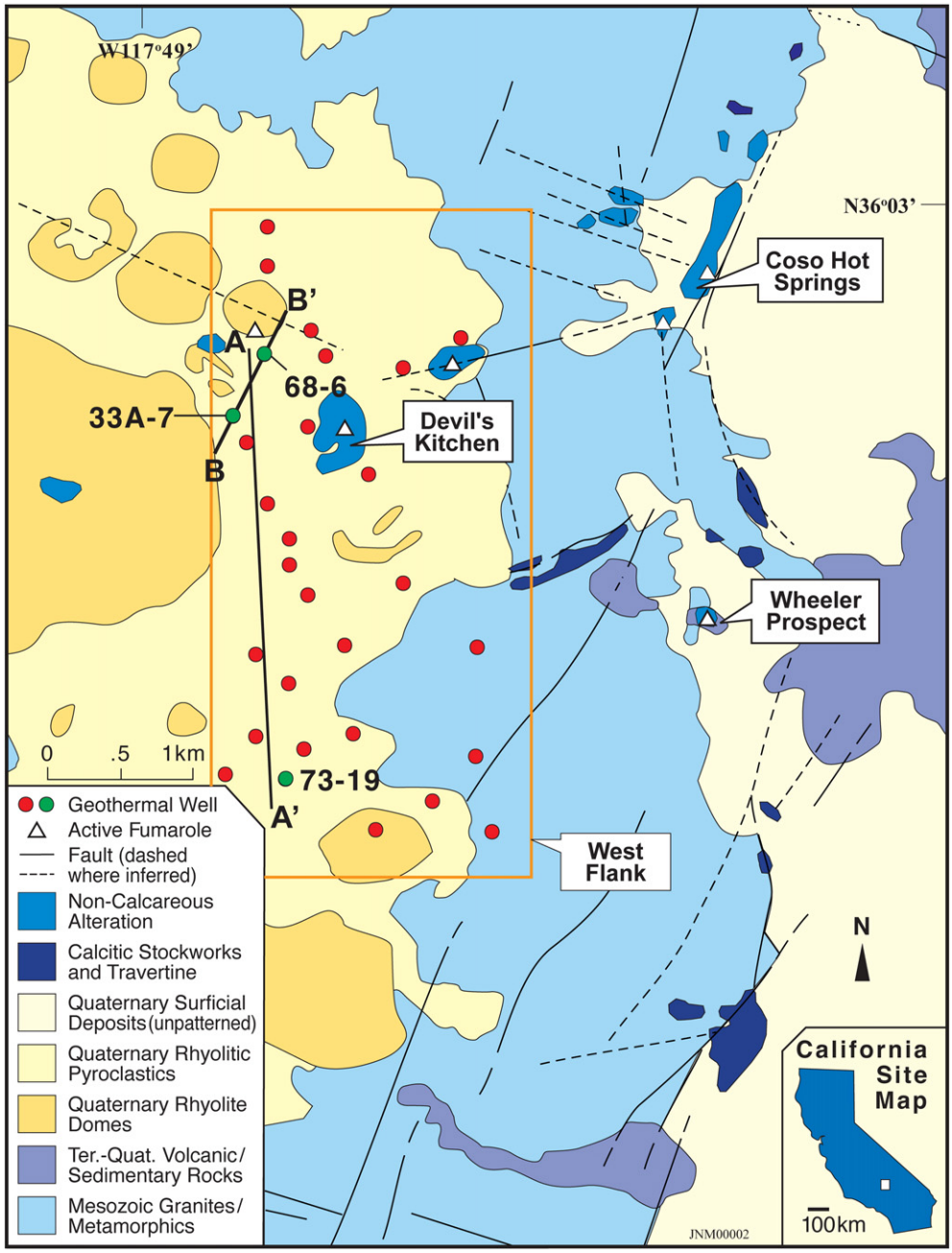

Fig. 1. A simplified geologic map of the Coso Geothermal system (modified from Hulen, 1978) located on the Naval Air Weapons Station, China Lake, California. The West Flank of the system is defined by a North-South trending thermal high; it is the focus of this study. Line A-A′ along this thermal high is the transect for a number of cross sections used in this study. Line B-B′ is a cross section line through wells 68-6 and 33A-7. Locations of wells in the West Flank used in this study are marked by red and green circles; the green circles indicate wells examined in detail for this study while the red circles indicate wells examined in previous studies. Only the wells in the West Flank with oxygen isotope data for host rocks are shown; none are shown for other areas.

and Gunderson, 1995; McConnell et al., 1997) and fossilized hydrothermal systems (e.g. Taylor, 1971; Taylor, 1973; Taylor, 1974; Forester and Taylor, 1980; Criss and Taylor, 1983; Larson and Taylor, 1986a; Larson and Taylor, 1986b; Faure et al., 2002; Mauk and Simpson, 2007). A number of these studies of fossil meteoric hydrothermal systems have demonstrated at least a qualitative correlation between increased $^{18}O/^{16}O$ depletion and the abundance of hydrothermal minerals, demonstrating that the extent of $^{18}O/^{16}O$ depletion can be a guide to the extent of fluid-rock interaction. In their studies of the active Long Valley hydrothermal system, both Smith and Suemnicht (1991) and White and Peterson (1991) noted that well cuttings from reservoir rocks (typically rhyolitic tuff with initial $\delta^{18}O_{wr}$ values of ~7.0‰) typically experience the greatest $^{18}O/^{16}O$ depletions (with $\delta^{18}O_{wr}$ values as low as −2.6‰) in the deeper, higher temperature parts of the system. Smith and Suemnicht (1991) also compared measured $\delta^{18}O_{wr}$ values to $\delta^{18}O_{wr}$ values calculated using then current measured temperatures, and demonstrated that many of their samples are out of oxygen isotope equilibrium with the current reservoir fluid at present temperature conditions. They concluded that this disequilibrium indicates that the Long Valley hydrothermal system has experienced protracted hydrothermal circulation at higher temperatures in the past. McConnell et al. (1997) utilized spatial patterns of $^{18}O/^{16}O$ depletion in well cuttings and core from reservoir rocks to define regional pathways of fluid circulation in the Long Valley Caldera hydrothermal system. Sturchio et al. (1990) noted the possible role of decompression boiling in producing oxygen isotope disequilibrium between current thermal waters and silica

minerals deposited in vugs and fractures in drill core samples from the Yellowstone geothermal system. Recently, Pope et al. (2016) measured δD and $\delta^{18}O$ values of hydrothermal epidote from the Krafla, Iceland geothermal system. They interpreted variations in the δD and $\delta^{18}O$ values of both the epidote and reservoir fluids to result from variable mixing of shallow, sub-boiling groundwaters with vapor condensates derived from an underlying two-phase reservoir, also derived from local meteoric waters.

In a previous study of the Coso geothermal system, Person et al. (2006) used $\delta^{18}O$ values of reservoir fluids and heat flow data to constrain a regional-scale numerical model of the flow system supplying the Coso geothermal system. In this study we report on oxygen isotope analyses of whole-rock samples from the Coso geothermal system, and detailed whole-rock and mineral analyses from three producing wells. Our whole-rock results identify discrete intervals of maximum $^{18}O/^{16}O$ depletion in the three wells that correspond closely with zones of current hot water production and high permeability. These discrete, higher permeability zones have experienced significant fluid infiltration, water-rock interaction and oxygen isotopic exchange with the geothermal fluids. Our results corroborate the results of a number of previous oxygen isotope studies of (mostly) fossil hydrothermal systems, and provide a particularly clear example of the connection between the extent of $^{18}O/^{16}O$ depletion, the extent of fluid-rock interaction and permeability in crystalline rock hosts to hydrothermal systems. Therefore mapping patterns of $^{18}O/^{16}O$ depletion can be another exploration tool to define permeability structure, identify higher permeability zones, and constrain fluid flow patterns—past and present—in active hydrothermal systems, and therefore help facilitate development of enhanced geothermal systems.

1.1. Geologic setting

The Coso Hot Springs geothermal system is developed in Mesozoic plutonic rocks of the Sierra Nevada Batholith (Duffield et al., 1980). Diorite that was regionally metamorphosed at greenschist to lower amphibolite facies conditions to orthogneiss in the late Cretaceous (Bartley et al., 2007) (Fig. 1) is the most common rock type. Younger intrusions consist of granodiorite and granite (Duffield et al., 1980). Subsequent episodes of Cenozoic volcanism produced basalt and rhyolite at 4.0–2.5 Ma and 1.1–0.044 Ma (Kurliovitch et al., 2003; Duffield et al., 1980). The youngest episode is related to a silicic magma chamber emplaced between 5 and 20 km depth (Duffield et al., 1980; Reasenberg et al., 1980; Manley and Bacon, 2000). This magma body produces the heat driving the current geothermal activity (Duffield et al., 1980).

Surface expressions of geothermal activity include opaline (SiO_2) sinter and travertine ($CaCO_3$) spring deposits. ^{14}C dating of pollen in hot spring deposits has yielded ages of 11,550 to 8550 years (Moore, unpublished data). The geothermal fluids (Table 1) have low salinities (5000–10,000 ppm TDS), and are NaCl-dominated. The pre-production geothermal waters are dominated by a single-phase system with minimal boiling (Fournier et al., 1980), but there is some mineral alteration evidence for a natural clay-rich steam cap in places (Williams and McKibben, 1990). Geochemical and hydrogen isotope data indicate that the system is predominately recharged by meteoric fluids (Adams et al., 2000; Moore et al., 1990; Williams and McKibben, 1990). The modeling results of Person et al. (2006) suggest that the geothermal fluids are recharged by lateral flow of groundwaters (meteoric waters) from fault systems and possibly the Sierra Nevada mountains to the west of the Coso field. Their model has these groundwaters infiltrating to the top of the brittle-ductile transition estimated at 4–5 km depth (Wilson et al., 2003), becoming enriched in $^{18}O/^{16}O$ to the maximum measured $\delta^{18}O$ values of the geothermal reservoir fluids (−6‰) through fluid-rock isotopic exchange at elevated temperature, and then ascending to form the thermal plume of the Coso reservoir. Northerly trending, Basin and Range faulting and local dextral strike-slip faulting associated with the younger Walker Lane/Eastern California Shear Zone, guide fluid flow and influence current geothermal activity (Monastero et al., 2005; Davatzes and Hickman, 2010; Kaven et al., 2012). Further, Davatzes and Hickman (2010) propose that stress-induced fracture slip leads to fluid flow and associated mineral alteration, which suggests that permeability will dynamically evolve as this system evolves over time. Additional details about the geology, including hydrothermal alteration, are provided by Hulen (1978), Duffield et al. (1980), Lutz et al. (1996), Adams et al. (2000), Manley and Bacon (2000), Kovac et al. (2005) and Etzel (2016).

Table 1
The composition of pre-production geothermal fluids from wells 68-6, 33A-7 and 73-19. Chemistry in ppm by weight; $\delta^{18}O$ and δD in per mil (‰) relative to VSMOW.

	68-6	33A-7	73-19
Na	748	1273	2044
K	136	187	579
Ca	7	7	50
Li	7	11	27
Mg	<1	N/A	N/A
B	39	58	89
SiO_2	596	514	602
HCO_3	102	124	44
SO_4	30	40	16
Cl	1260	2163	3783
F	3	3	2
$\delta^{18}O_W$	−8.5‰	−7.5‰	−6.0‰
δD	−104‰	N/A	−96‰
Date measured	6/26/1995	7/28/2009	10/26/1988

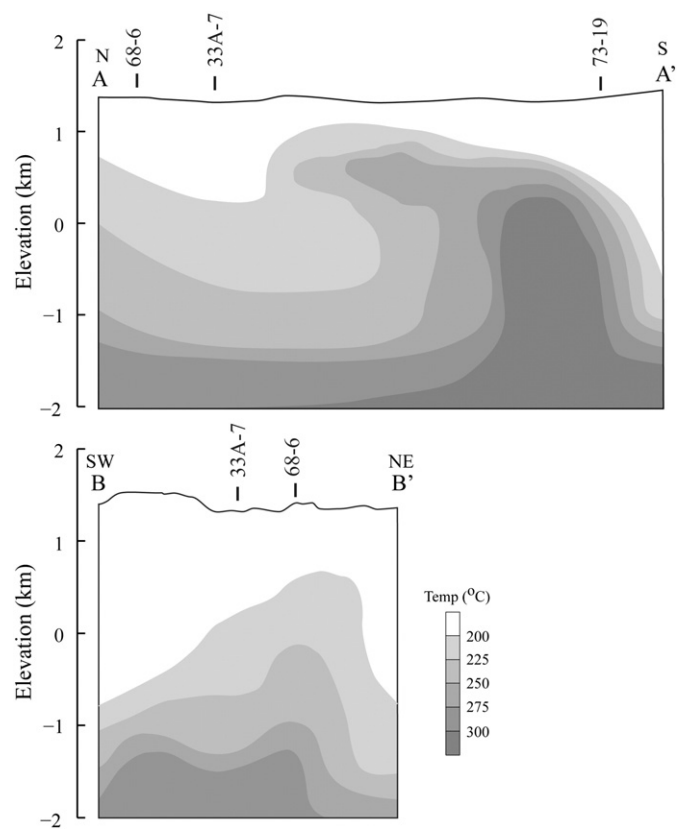

Fig. 2. General north-south thermal structure of the West Flank along the transects A-A′ and B-B′. Temperature values come from down-hole measurements made prior to production. Only wells 68-6, 33A-7 and 73-19 are shown for reference; in total, thermal data from 25 wells in the West Flank were used to construct these cross-sections. Measurements are available to elevations approaching −2 km in almost all of these wells; therefore, these temperature contours are well constrained at all depths displayed.

1.2. Thermal structure

Borehole measurements have defined a north-south trending zone of high temperatures on the West Flank of the field (Fig. 1). Geochemical and thermal data suggest that the system is compartmentalized with upflow zones in the northeast and southwest (Williams and McKibben, 1990). Fig. 2 shows the thermal structure of the West Flank of the system based on pre-production temperature data. Maximum measured temperatures at depth reach 350 °C. Reservoir temperatures in the south are higher than in the north at equivalent elevations. The thermal pattern defines a plume of hot water that ascends in the south and then migrates laterally northward.

2. Methods

Rock cuttings were sampled at regular intervals (nominally ~30–80 m apart) in wells 68-6, 33A-7 and 73-19 for oxygen isotope, X-ray diffraction (XRD) and petrographic analyses. Thin sections were examined using a petrographic microscope under transmitted light to identify primary and secondary (alteration) minerals, vein mineral assemblages and their paragenesis, structural features and the host rock lithology. Etzel (2016) provides a detailed presentation of these results.

Clay mineralogy and clay mineral abundances have been determined by X-ray diffraction analyses of whole-rock and clay-size fractions (<5 μm) at the Energy & Geosciences Institute at the University of Utah, using a Bruker D8 Advance X-ray diffractometer. The clay mineralogy was determined using methods described by Moore and Reynolds (1997) on air-dried and glycolated scans of the clay-sized fraction. Phase quantification using the Rietveld method was performed using TOPAS software, developed by Bruker AXS, as described in Lutz and Moore (1997). Mineral abundances are in weight percent with values rounded to the nearest whole number. Values of less than one weight percent obtained from Rietveld analysis are reported as trace amounts. Additional details of these techniques, clay mineralogy and of host rock lithology are reported in Etzel (2016).

Oxygen isotopic measurements were conducted at the University of Wisconsin-Madison on 91 whole rock samples and 30 feldspar separates from wells 68-6, 33A-7 and 73-19. Mineral separates were made using a Frantz magnetic separator followed by hand-picking under a stereoscopic microscope. The oxygen isotope analyses were done by laser-aided fluorination using a lasing sample chamber outfitted with an airlock sample chamber to prevent pre-fluorination of reactive rock powders (Spicuzza et al., 1998). Oxygen isotope values are reported in the standard $\delta^{18}O$ notation, relative to VSMW, and are standardized using UWG-2 garnet ($\delta^{18}O = 5.8‰$; Valley et al., 1995). Multiple analyses of UWG-2 ($n > 4$) within individual analytical sessions yield a reproducibility of $\pm 0.07‰$ (2σ). The average measured $\delta^{18}O$ values for all analyses of UWG-2 done in this study ($n = 34$) is $5.71 \pm 0.20‰$ (2σ), within error of the published value for this standard. The 513 whole rock oxygen isotope analyses made available by Terra-Gen were analyzed at Southern Methodist University. These oxygen isotope analyses were determined using the bromine pentafluoride extraction procedure described by Clayton and Mayeda (1963). The $\delta^{18}O$ analyses are reported relative to VSMOW, and long-term analyses of in-house standards indicate reproducibility of $\pm 0.2‰$.

Isotopic measurements of the geothermal fluid (Table 1) were also made at Southern Methodist University and are reported relative to VSMOW. For oxygen, isotopic compositions were determined following a method similar to that of Epstein and Mayeda (1953) and hydrogen oxygen isotope compositions were determined following a method similar to what was described by Bigeleisen et al. (1952). In-house standards indicate a long term reproducibility of $\pm 0.1‰$ for $\delta^{18}O$ and $\pm 1‰$ for δD. The $\delta^{18}O$ values of the pre-production reservoir fluids (Table 1) were determined using measured temperature, pressure and $\delta^{18}O$ values of the separated vapor (steam) and liquid water sampled during

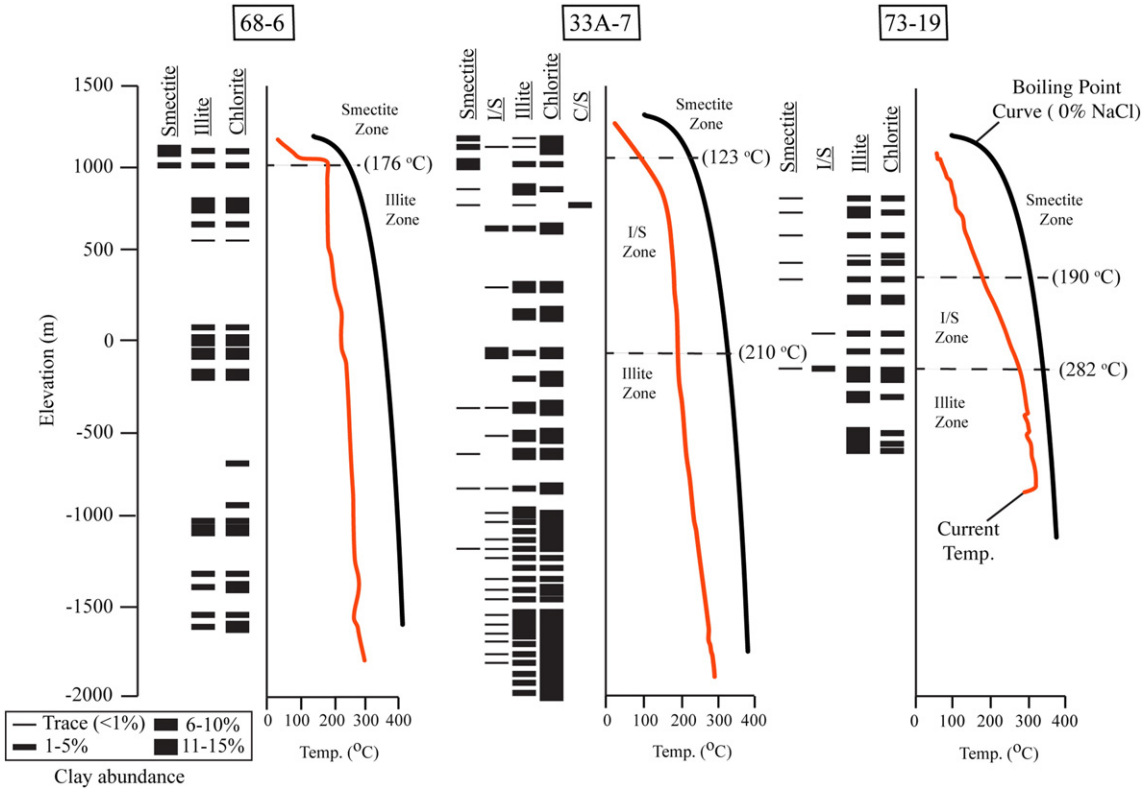

Fig. 3. Clay mineral content and measured pre-production temperature profiles for wells 68-6, 33A-7 and 73-19. I/S = interlayered illite-smectite; C/S = interlayered chlorite-smectite. Dashed lines denote locations at which clay transitions occur; measured temperatures at these locations are in parentheses. Boiling point curves calculated following the approach presented by Haas (1971).

pre-production flow tests in each, following the heat and mass balance calculations described by Truesdell (1984).

3. Results

3.1. Host rock and alteration mineralogy

The reservoir rocks observed in wells 68-6, 33A-7 and 73-19, the three wells studied in detail (well locations shown in Fig. 1) are principally diorite orthogneiss with subordinate diorite and granodiorite.

Two episodes of overprinting on the primary (igneous) mineralogy of the reservoir rocks are recognizable (Bishop and Bird, 1987; Lutz et al., 1996; Lutz and Moore, 1997; Kovac et al., 2005; Etzel, 2016). Regional lower amphibolite to greenschist facies metamorphism (late Cretaceous) has produced plagioclase, hornblende, biotite, epidote, titanite, chlorite and illite (muscovite) throughout all three wells (Figs. 3, 4a, b). During subsequent geothermal activity, chlorite and rare interlayered smectite/chlorite replaced hornblende and biotite, and epidote, illite (muscovite) and other clay minerals replaced plagioclase (Fig. 4c–f). This geothermal activity has resulted in progressive changes in temperature sensitive clay minerals with depth. Throughout the field, smectite (S) is present at the shallowest depths, followed by interlayered illite/smectite (I/S) and rare chlorite/smectite, and finally illite and chlorite at deeper levels.

The deepest occurrence of smectite above trace levels (>1 wt%) defines the base of the smectite zone at an elevation of about 1000 m in wells 68-6 and 33A-7 (Fig. 3). In well 73-19, smectite occurs only at trace levels (<1 wt%) and occurs persistently only at elevations above ~300 m (Fig. 3). The deepest occurrence of interlayered illite-smectite above trace levels defines the base of the I/S zone in wells 33A-7 and 73-19 at elevations of −41 m and −143 m, respectively. Interlayered illite-smectite is completely absent in well 68-6. Trace amounts of the lower temperature smectite and interlayered I/S clays exist within the illite zone in 33A-7 (Fig. 3).

The transitions from smectite to interlayered illite/smectite to illite typically occur at temperatures of ~180 °C and 225 °C, respectively (Steiner, 1968; Browne, 1978; Henley and Ellis, 1983; Browne, 1984; Reyes, 1990). However, in the three Coso wells, these transitions do not always occur at or near these temperatures, based on measured pre-production temperatures in wells (Fig. 3). In 33A-7, the smectite to interlayered illite/smectite and illite/smectite to illite transitions occur well below expected temperatures at ~123 °C and ~210 °C, respectively. In well 73-19, the smectite to interlayered illite/smectite transition occurs near the expected T of 180 °C, but interlayered illite/smectite persists to depths where temperatures exceed 280 °C. In 68-6 smectite disappears near a pre-production temperature of 180 °C (at an elevation of ~1000 m), its expected limit of thermal stability, but no interlayered illite/smectite is present below the smectite. These discrepancies suggest that temperature variations alone cannot explain the detailed distribution of clay minerals observed in these wells.

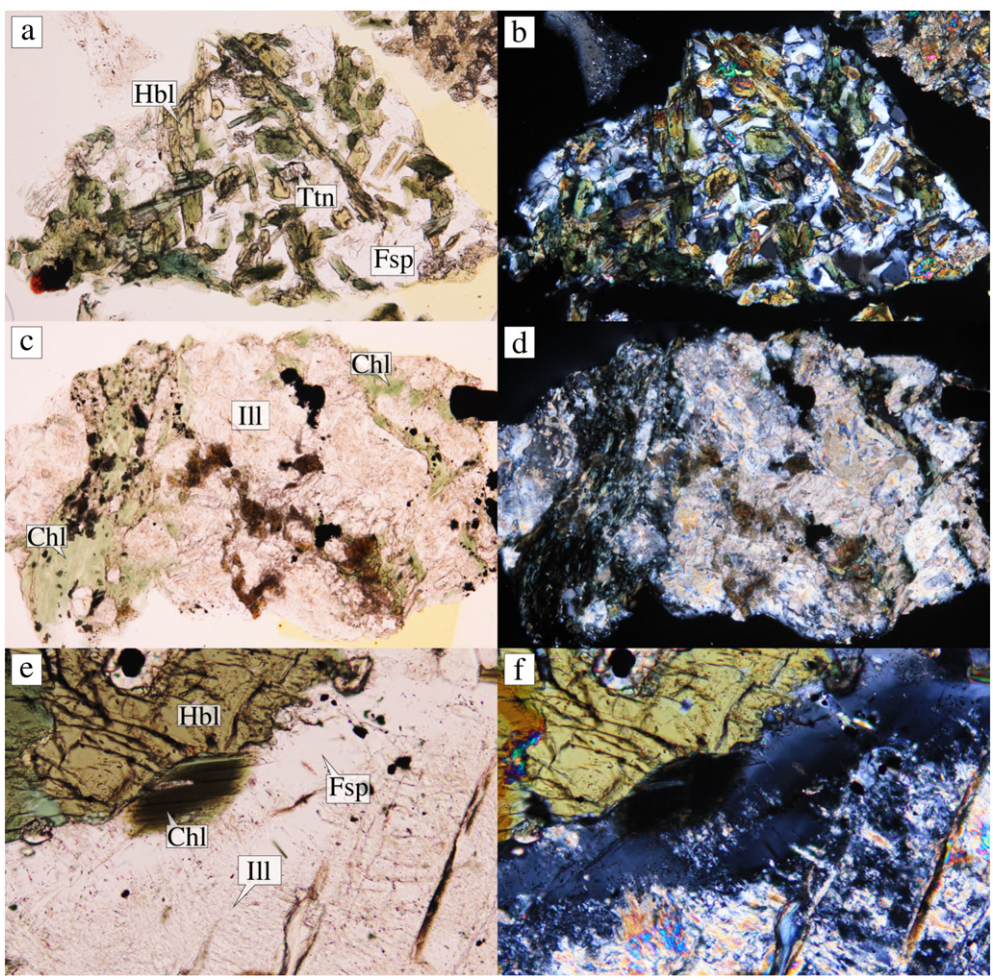

Fig. 4. Photomicrographs of the lithologies and alterations observed in the Coso geothermal system. Panels a) and b) show a typical unaltered meta-diorite sample with hornblende (Hbl), untwined feldspar (Fsp), and rare anhedral titantite (Ttn). This sample is from 33A-7_1100. Panels c) and d) show extensive geothermal-related alteration in feldspar, hornblende and biotite found in 68-6_2792. Feldspar is altered to illite (Ill); hornblende and biotite are completely altered to chlorite (Chl). Panels e) and f) show a feldspar partially altered to illite found in 68-6_2941. The field of view in panels a) – d) is 1.6 mm and in panels e) and f) is 0.8 mm.

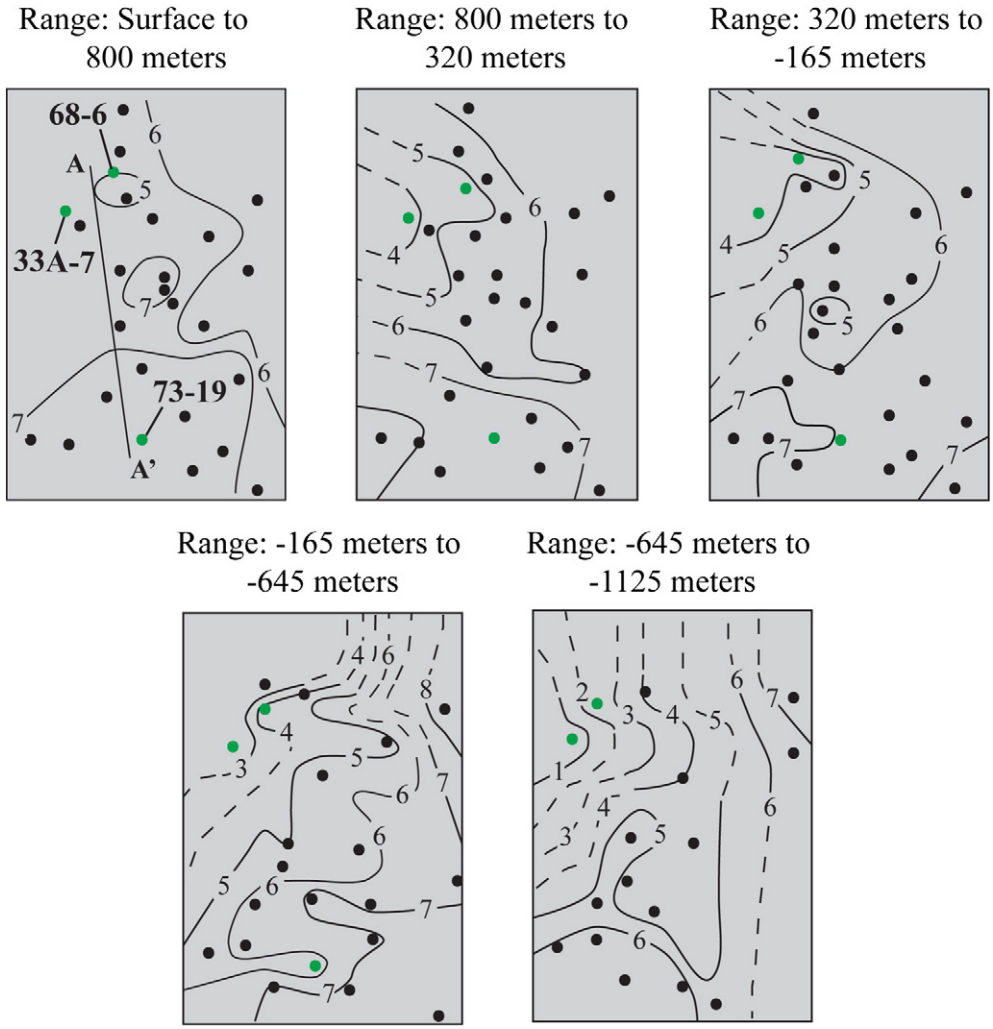

Fig. 5. Contoured plan maps of the whole rock oxygen isotope data at a series of elevation intervals in the Coso system. The area of each slice is equal to the area of the West Flank outlined in Fig. 1 but the horizontal dimension has been exaggerated for visual clarity. On each map, the $\delta^{18}O$ values for each well location are the average of all $\delta^{18}O$ data from that well within the 480 m elevation interval represented by that map. The contour values are in ‰. Dashed lines are used where contouring has been inferred. All elevations are relative to sea level. The green and black dots are well locations; green dots are wells 68-6, 33A-7 and 73-19. The location of transect A-A′ in the West Flank is shown in the upper left panel. Contours were generated using the MATLAB contour function.

3.2. Whole rock oxygen isotope characteristics of the Coso Hot Springs geothermal system

General patterns of $\delta^{18}O$ variation as a function of elevation in the West Flank of the Coso geothermal field are illustrated in Fig. 5. These plan contour maps are based on 513 whole rock $\delta^{18}O$ analyses of well-cuttings supplied by Terra-Gen Operating Company (Supplementary Data Table A.1), plus 91 additional whole rock $\delta^{18}O$ values measured in this study (Table 2). The plan maps of $\delta^{18}O$ variations shown in Fig. 5 were constructed by averaging the $\delta^{18}O$ values within 480 m intervals in each well; sufficient analyses were not available deeper than 1125 m below sea-level to construct a useful plan map. Contouring was done using the MATLAB contour function. This function requires position (in this case we used northing and easting values recorded during drilling) and a calculated average $\delta^{18}O$ value within each interval for each well used. Average $\delta^{18}O$ values used for contouring are presented in Supplementary Data Table A.3. Near surface $\delta^{18}O$ values (surface to 800 m elevation) are similar with, or slightly lower than, measured $\delta^{18}O$ values for primary igneous rock in the Central Sierra Nevada Batholith (+7.5‰ to +9.0‰; Masi et al., 1981; Lackey et al., 2008) except for depletion to $\delta^{18}O$ values between +5‰ and +6‰ in the northwest quadrant of the system.

With increasing depth, significant and widespread decreases in $\delta^{18}O$ occur only in the northwest quadrant, where $\delta^{18}O$ values can decrease down to values between 0 and +1‰ (−645 to −1125 m elevation interval). Regardless of depth, the host rock in most of the southern half of the reservoir does not experience significant $^{18}O/^{16}O$ depletion below +5‰. At the sampling scale of Fig. 5, the thermal upflow zones inferred in the SW and NE sectors of the field by Williams and McKibben (1990) are not reflected in significant lowering of $\delta^{18}O$ values in these sectors.

Fig. 6 illustrates variations in whole rock $\delta^{18}O$ values within the vertical section A-A′ shown in Fig. 1 (along the West Flank). Again, contouring with a MATLAB contour function, but using all whole rock $\delta^{18}O$ values (no averages). In general, depletions in $^{18}O/^{16}O$ are more extensive and extend to significantly greater depth in the northern portion of the cross-section. In detail, localized intervals of significant $^{18}O/^{16}O$ depletion, with less depleted rocks above and below, occur in the northern wells 68-6 and 33A-7 in intervals centered on elevations of 200, −200 and −1200 m. Maximum depletions to $\delta^{18}O$ values below 0‰ occur in the lowest of these intervals. In contrast, host rocks in the southern part of the traverse are not significantly depleted except for two or three discrete intervals in 73-19 and 58A-18. These spatial patterns of localized and significant ^{18}O depletions do not reflect the spatial $\delta^{18}O$ patterns expected from the low and smooth temperature gradients (dT/dx) characteristic of regional metamorphism. The

Table 2
Measured $\delta^{18}O$ values for whole rock and feldspar mineral samples from well 68-6, 33A-7 and 73-19, Coso geothermal system, California. Values are reported in per mil (‰) notation, relative to VSMOW. Elevation is in meters above sea level (msl).

Well: 68-6			Well: 33A-7			Well: 73-19		
Elevation (m)	Whole-rock (‰)	Feldspar (‰)	Elevation (m)	Whole-rock (‰)	Feldspar (‰)	Elevation (m)	Whole-rock (‰)	Feldspar (‰)
996	3.88		1251	7.62	7.50	996	6.98	7.79
937	4.47	6.04	1175	3.70		886	6.61	
855	2.55		1023	5.39		877	6.37	
789	3.49	6.59	870	7.45		822	7.48	8.12
710	5.08		718	4.84		722	5.52	
587	5.78		639	5.34		490	7.57	
556	6.02	6.29	413	0.20		469	6.36	
394	3.57		261	3.59		207	7.16	
293	4.07		185	3.00	5.49	195	7.41	
208	4.30		−41	4.18		42	6.07	
31	4.43		−283	3.89		−49	6.63	
−60	2.44	5.24	−360	2.71		−79	5.91	
−129	2.87		−585	1.03		−119	4.61	6.14
−165	1.50	4.96	−689	3.93		−143	2.38	
−230	2.60		−833	1.60		−213	6.30	7.26
−365	3.78	5.64	−904	−0.44		−313	5.94	
−455	4.67	6.76	−1005	−0.02		−395	6.85	
−581	4.46		−1005	−1.02		−441	5.13	
−707	2.94		−1031	−0.98		−544	5.14	6.20
−911	2.70		−1059	0.14		−565	3.30	6.34
−1020	0.75		−1114	0.51	−2.37	−586	3.30	
−1091	0.75	3.09	−1170	−2.35				
−1188	0.61		−1195	−3.08	−0.03			
−1327	0.75	3.08			+0.63[a]			
−1407	2.83	3.59	−1230	0.94	4.16			
−1463	0.54		−1284	2.15	4.20			
−1511	0.26		−1314	1.55				
−1552	−4.60	−3.88	−1343	2.92				
		−5.06[b]	−1230	2.10	4.60			
		−4.12[a]	−1402	3.91				
−1594	−1.05	1.76	−1487	4.48	5.49			
−1706	0.64		−1603	4.60				
			−1632	4.25				
			−1661	4.05				
			−1690	1.78				
			−1721	4.21				
			−1751	4.03				
			−1782	4.61				
			−1812	4.10				
			−1873	4.49				
			−1934	3.88	5.90			

[a] Feldspar separated from finer-grained (150–200 mesh) whole rock aliquot.
[b] Hand picked cloudy (more altered) feldspar.

observed spatial patterns of $\delta^{18}O$ variation are instead more consistent with localized ^{18}O depletions expected from fluid-rock interactions related to discrete zones of high permeability associated with geothermal activity.

The thermal structure along the cross-section A-A′ (Fig. 2) is also superimposed on this $\delta^{18}O$ cross-section in Fig. 6 which shows that variations in pre-production temperatures are not, in general, well correlated with variations in whole-rock $\delta^{18}O$ values. With the few localized exceptions noted above, the host rocks are not depleted in $^{18}O/^{16}O$ to any significant extent in the southern part of the traverse, even within the deeper, higher temperature levels. In the northern part of the section, hotter host rocks below −1400 m are less depleted in $^{18}O/^{16}O$ than cooler rocks immediately above between −1000 and −1400 m. However, depth intervals of current production in all three wells do correlate with zones of maximum $^{18}O/^{16}O$ depletion (Fig. 6). This correlation suggests that permeability plays an important role in controlling the extent of fluid-rock interaction—and hence the extent of $^{18}O/^{16}O$ depletion—experienced by the host rocks in the Coso geothermal system.

3.3. Oxygen isotope characteristics of the west flank

3.3.1. Whole rock $\delta^{18}O$ analyses

Wells 68-6, 33A-7 and 73-19 were selected for detailed oxygen isotope analyses of whole-rock and mineral separates (Table 2; Fig. 7). In well 68-6 (Fig. 7a) whole-rock $\delta^{18}O$ values are somewhat to moderately depleted in $^{18}O/^{16}O$ relative to primary igneous values (+7.5 to 9.0‰), and fluctuate between 1.8‰ and +6.0‰ down to ~−700 m elevation, with a tendency to decrease with depth. Below −700 m, $^{18}O/^{16}O$ depletions are even greater, and the maximum $\delta^{18}O$ value is +3.0‰, with most $\delta^{18}O$ values below +1‰. Whole rock $\delta^{18}O$ values reach a minimum of −4.6‰ at −1552 m above sea level (msl) (Fig. 7a). In well 33A-7 $\delta^{18}O$ values generally decrease with elevation from a maximum value of +7.6‰ at an elevation of 1251 m to a minimum of −3.1‰ at −1195 m, just above the production zone (interval of lost circulation) in the well (Fig. 7b). Immediately below, and to the bottom of the well, $\delta^{18}O$ values are significantly higher, ranging between +3 to +4.9‰, but are still significantly lower than primary igneous values. The host rocks in well 73-19 are less depleted in $^{18}O/^{16}O$ compared to the rocks of the other two wells (Fig. 7c). The highest measured $\delta^{18}O$ values from whole rock samples overlap primary igneous $\delta^{18}O$ values of +7.5 to 9.0‰ (Masi et al., 1981; Lackey et al., 2008). The only $\delta^{18}O$ values below +5‰ occur at elevations of −119 m and below. The minimum $\delta^{18}O$ value in well 73-19 is still positive, +2.4‰ (−143 m elevation, Fig. 7). In all three wells, samples with the lowest measured $\delta^{18}O$ values (or with $\delta^{18}O_{wr} \leq 2.0$‰, well 33A-7) correspond with major intervals of lost circulation, the primary production intervals for each well (Fig. 7).

3.3.2. Feldspar vs. whole rock oxygen isotope compositions

Measured $\delta^{18}O$ in bulk feldspar separates range from 6.8‰ to −3.9‰ in well 68-6 and from 7.5‰ to −2.4‰ in 33A-7; feldspars

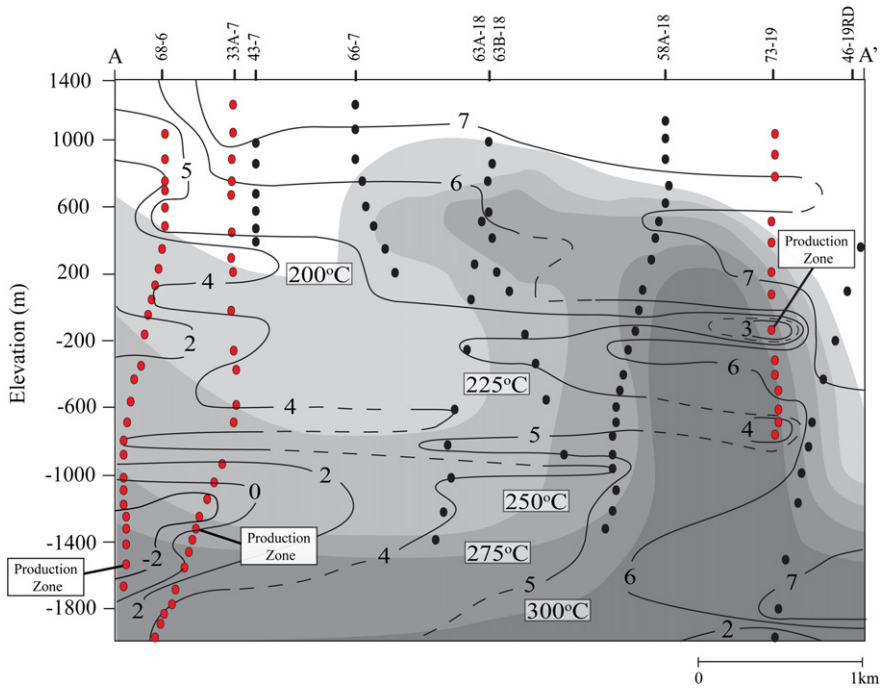

Fig. 6. Vertical cross section of the whole rock oxygen isotope data along the north-south transect, A-A′. The locations of the nine wells on or close to the A-A′ traverse (Fig. 1), and data points from each well used for contouring $\delta^{18}O$ values are shown; contours are in ‰. Red circles indicate the locations of samples analyzed in this study. Isotherms based on preproduction downhole measurements from Fig. 2 are superimposed to define areas along the cross section above 300 °C (dark gray) and between 200 °C and 300 °C in varying shades of gray; see text for discussion. The major production zone in each well is noted.

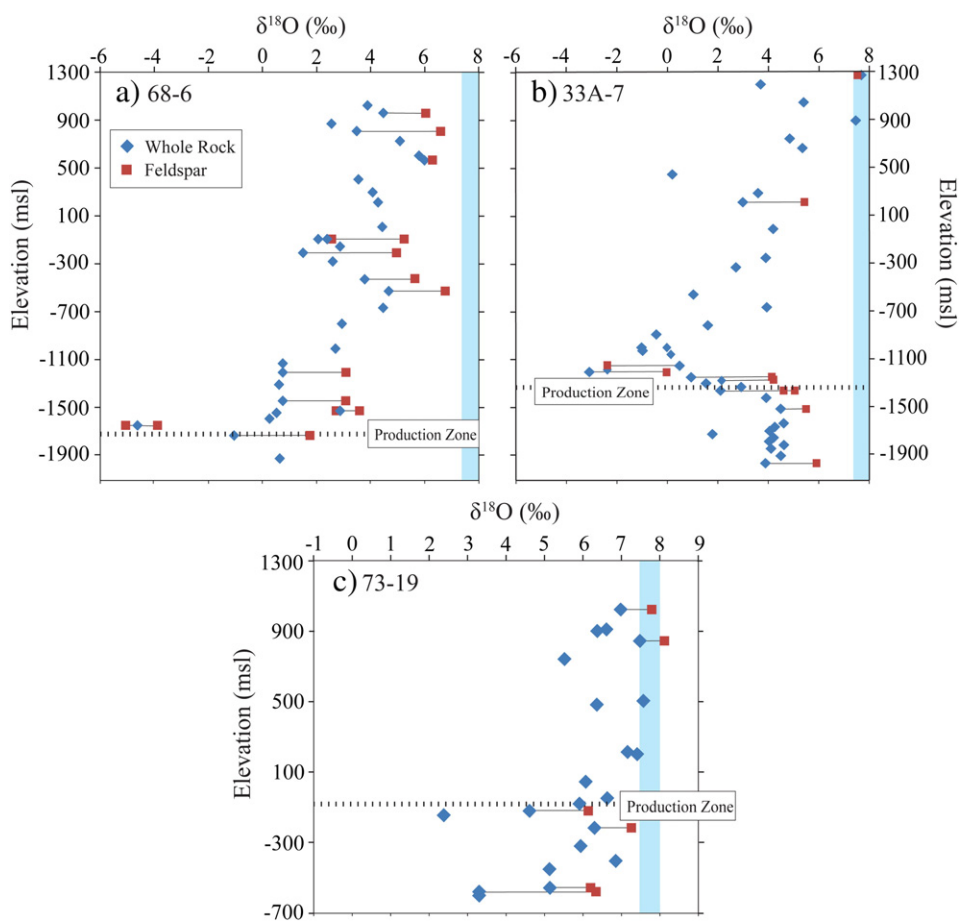

Fig. 7. Measured $\delta^{18}O$ values of whole rock and feldspar samples as a function of elevation for well 68-6 (panel a), 33A-7 (panel b) and 73-19 (panel c). All values are reported in per mil (VSMOW), and plotted at elevation (meters above sea level). The shaded light blue regions represent the range of primary $\delta^{18}O$ values of diorite to granodiorite rocks from the region that are equivalent to the reservoir host rocks in the Coso system (Lackey et al., 2008). The dotted line marks the current production zone (interval of lost circulation) in each well.

from well 73-19 have higher $\delta^{18}O$ values ranging from 8.1‰ to 6.1‰. In all three wells, the $\delta^{18}O$ values of the feldspar correlate positively with the whole-rock $\delta^{18}O$ values, and are systematically 1 to 3‰ higher than the whole rock values, even in the more $^{18}O/^{16}O$-depleted samples (Fig. 7a). The only exception is in 33A-7 at −1139 msl. The bulk feldspar separates are mixtures of primary (igneous or metamorphic) feldspar and feldspar that has experienced oxygen isotope exchange with geothermal fluid (hydrothermal feldspar). The hydrothermal feldspar should have a considerably lower $\delta^{18}O$ value than primary feldspar, owing to the low $\delta^{18}O$ value of the geothermal fluid and intermediate temperature of exchange (≤350 °C). Further, feldspar is normally more susceptible to oxygen isotope exchange compared to hornblende and less abundant quartz in the host diorite and quartz diorite (Taylor and Forester, 1979; Criss and Taylor, 1983; Cole et al., 1992). As a result, hydrothermal feldspar might be expected to have a $\delta^{18}O$ value less than that of the whole-rock for rocks that are only moderately depleted in $^{18}O/^{16}O$. In thin section, primary igneous and regional metamorphic feldspar are clear and twinned (igneous feldspar); hydrothermal feldspar is cloudy and sometimes turbid from the presence of pits/cavities and very small grains of clay minerals. The intergrown nature of primary and hydrothermal feldspar at the grain scale makes their effective separation by standard density means impractical. However, a concentrate of cloudy-looking feldspar was made by hand picking the bulk feldspar separate from sample 68-6_-1552. Analysis of this concentrate yielded a $\delta^{18}O$ value of −5.1‰, significantly lower than the bulk feldspar (−3.9‰) and whole rock (−4.6‰) $\delta^{18}O$ values of this sample (Table 2). In-situ (SIMS) analysis will be necessary to define clearly the $\delta^{18}O$ value of hydrothermal feldspar in the host rock (e.g., Valley and Graham, 1996; Valley and Kita, 2009). Regardless, this systematic difference between measured $\delta^{18}O$ values of bulk feldspar and whole rock suggests that the $\delta^{18}O$ values of both feldspar and whole rock reflect the extent of interaction (and oxygen isotopic exchange) between host rock and geothermal fluid.

Another possibility for the systematic $^{18}O/^{16}O$ enrichment in bulk feldspar relative to the whole rock is that the lower $\delta^{18}O$, hydrothermally altered feldspar was preferentially removed by crushing during preparation of the sample aliquots (>80 or >100 mesh size) from the whole rock used to make plagioclase separates. To test this possibility, additional analyses were made of feldspar separated out of the finer-grained (150 to 200 mesh) residual fraction of the whole rock aliquots for two samples. The analyzed $\delta^{18}O$ values for these finer-grained feldspar separates are −4.1‰ (compared to −3.9) for sample 68-6_-1551, and +0.6‰ (compared to −0.0‰) for sample 33A-7_-1195 (Table 2). Additional details of these results are in Etzel (2016). Feldspar separates from these finer-grained fractions are not significantly lower in $\delta^{18}O$ compared to feldspar separates from the coarser-grained fractions.

The systematically higher measured $\delta^{18}O$ values of feldspar relative to the whole rock indicate, from mass balance considerations, that there is at least one other major phase (likely chlorite and/or other clay mineral alteration products) in the rock that is significantly depleted in $^{18}O/^{16}O$ relative to the whole rock value. Chlorite can replace hornblende but would be stable with biotite during the greenschist facies conditions of the earlier regional metamorphism; this generation of chlorite will not be related to geothermal activity. Replacement of biotite by chlorite would more likely occur at the sub-greenschist facies conditions of the geothermal environment. Hence, bulk separates of chlorite will potentially contain two generations of chlorite of very different $\delta^{18}O$ value. Good separation of bulk samples of chlorite by magnetic and density methods proved impractical owing to the intergrowth of chlorite with biotite and hornblende at the grain size scale. Concentrates of chloritized biotite from four samples were handpicked. Their $\delta^{18}O$ values, compared to whole rock values (in parentheses) are: 1) 0.2‰ (3.8), sample 68-6_-382; 2) −3.2‰ (0.7), sample 68-6_-911; 3) −3.8‰ (−3.1), sample 33A-7_-1195; and 4) −0.45‰ (4.6), sample 73-19_-119. These chloritized biotites are from almost 1 to as much as 5‰ depleted in $^{18}O/^{16}O$ relative to the whole rock values, satisfying at least qualitatively this mass balance requirement. In-situ analyzes will be necessary to define the $\delta^{18}O$ values of the hydrothermal chlorite more precisely.

4. Discussion

4.1. Clay mineralogy as a function of fluid-rock interaction

The observed distributions of clay minerals in wells 68-6, 33A-7 and 73-19 are inconsistent with the pre-production temperatures in these wells (Fig. 3). These discrepancies may indicate that the pre-production thermal regime was different than the regime responsible for clay mineral zoning, and that the clay minerals have not yet re-adjusted to the newer (pre-production) thermal conditions. The persistence of clay minerals outside their normal stability fields (e.g., smectites at T > 180 °C in 73-19, Fig. 3) is common but the reasons are poorly understood. Nucleation and reaction kinetics may play roles. Permeability, which can either promote (high permeability) or inhibit (low permeability) clay-fluid interactions, may also be influencing the spatial distribution of the clay minerals.

Oxygen isotope evidence suggests that the extent of fluid-rock interaction experienced by the host rock is influencing the distribution of clay minerals in the Coso system. The amount of $^{18}O/^{16}O$ depletion is a monitor of the extent of fluid-rock interaction by the host rock—and hence it's permeability. Fig. 8 superimposes the distribution of clay minerals in wells 68-6, 33A-7 and 73-19 on variations in whole rock $\delta^{18}O$ values along the cross section A-A′. The host rocks are systematically more depleted in $^{18}O/^{16}O$ at depth at the north end compared to the south end of the traverse. In addition, significant $^{18}O/^{16}O$ depletions extend to markedly shallower depth at the north end of A-A′. The overall extent of $^{18}O/^{16}O$ depletion in the south third of the traverse is considerably less, and significant $^{18}O/^{16}O$ depletions in well 73-19 are confined to several discrete/narrow/short intervals. Hence in well 73-19 the transition from smectite to interlayered illite/smectite clay is better correlated with temperature, as this transition occurs near the expected temperature of 180 °C (Fig. 3). However, interlayered illite/smectite clay occurs as deeply as −143 m elevation (T = 282 °C, Fig. 3) in well 73-19, an elevation corresponding to a local interval of significant $^{18}O/^{16}O$ depletion ($\delta^{18}O$ < 4‰). Fig. 6 shows that there is a general correlation between greater and more spatially widespread $^{18}O/^{16}O$ depletion in the north end of A-A′ with a thinner smectite zone in 68-6 and 33A-7 and the lack of a mixed illite/smectite transition zone in 68-6. Additionally, the transition from interlayered illite/smectite to illite clay in 73-19 is correlated with local $^{18}O/^{16}O$ depletion. These highly $^{18}O/^{16}O$ depleted zones within traverse A-A′ record greater fluid-rock interaction, and are characterized by higher permeability based upon the greater extent of $^{18}O/^{16}O$ depletion relative to other portions of the reservoir. Hence the extent of fluid-rock interaction (host rock permeability) appears to be controlling, at least in part, the spatial distribution of clay minerals and clay zoning patterns in wells 68-6, 33A-7 and 73-19 along the traverse A-A′.

4.2. Oxygen isotope exchange and fluid-rock interaction

The $\delta^{18}O$ values of the whole rock samples from the West Flank range widely from −4.6‰ to 7.6‰ (Table 2). Reservoir rocks in 33A-7 and 68-6, except for the shallowest levels, have experienced at least moderate $^{18}O/^{16}O$ depletions ($\delta^{18}O$ < 5.0‰) from primary igneous $\delta^{18}O$ values (+7.5 to 9.0‰; Lackey et al., 2008). Hence most of the reservoir rock sampled in these two wells has experienced at least some interaction and oxygen isotope exchange with the geothermal reservoir fluid derived from low $\delta^{18}O$ local meteoric water. Further, a few discrete intervals in 33A-7 and 68-6 have experienced significantly greater $^{18}O/^{16}O$ depletion, and have negative whole-rock $\delta^{18}O$ values ranging as low as −4.6‰.

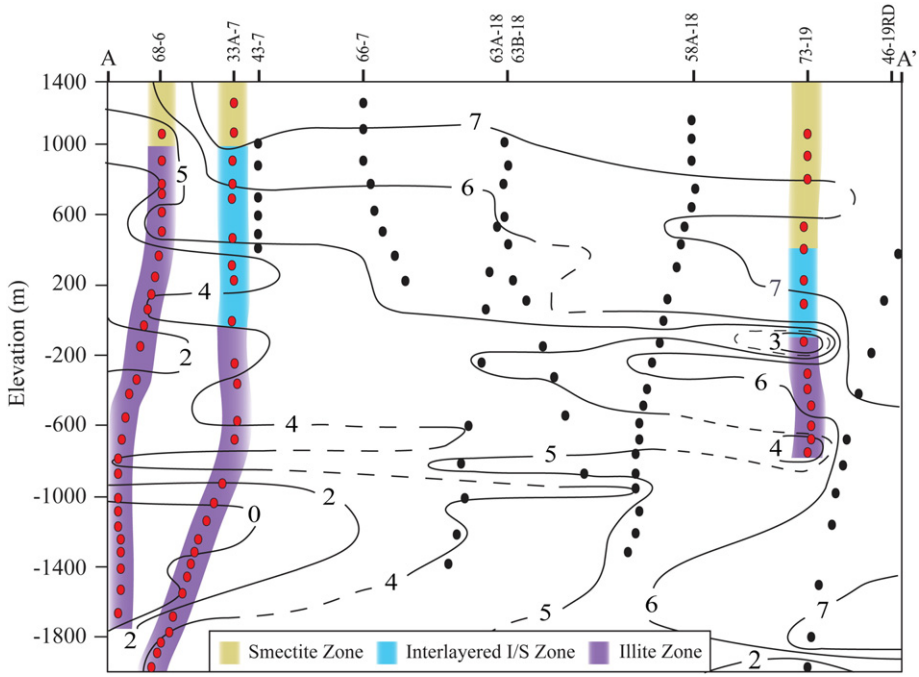

Fig. 8. Clay zones within wells 68-6, 33A-7 and 73-19 superimposed onto the contoured cross-section of $\delta^{18}O$ values along the traverse A-A′ in the West Flank. Black circles represent intervals with preexisting $\delta^{18}O$ values, red circles represent intervals where $\delta^{18}O$ values were determined for this study. Increasing extent of $^{18}O/^{16}O$ depletion northward correlates with changes in clay mineral zoning with depth, suggesting a correlation between clay mineral stability, extent of fluid-rock interaction and permeability (see text for discussion).

Significant variations in the extent of $^{18}O/^{16}O$ depletion have been documented in other active hydrothermal systems, such as the system at Long Valley, CA, where in general, rock samples from deeper and higher T sections of wells tend to have lower $\delta^{18}O$ values (Smith and Suemnicht, 1991; White and Peterson, 1991). Both these studies and McConnell et al. (1997) attribute these large-scale variations in $\delta^{18}O$ values primarily to variations in temperature—both spatially and over time. In the West Flank at Coso, the $\delta^{18}O$ values generally decrease in well 33A-7 with increasing depth (and increasing T) down to the production zone (Fig. 7), so temperature is likely playing a role in determining the extent of $^{18}O/^{16}O$ depletion at large spatial scales in the Coso system as well. These previous studies at Long Valley also document smaller-scale variations in the extent of $^{18}O/^{16}O$ depletion that they attribute to incomplete exchange (either from kinetic barriers or limited permeability), or to varying abundances of less easily and more easily altered minerals/rock components in the samples analyzed (McConnell et al., 1997). In the three wells analyzed at Coso in this study, localized intervals of significantly greater $^{18}O/^{16}O$ depletion than in rocks immediately above or below (Fig. 7) indicate that these reservoir host rocks have experienced significant variations in the extent of fluid-rock interaction.

The extent of $^{18}O/^{16}O$ depletion is a function of the amount of reservoir fluid with which the rock has interacted, the temperature and the degree to which isotope exchange equilibrium is attained. Box model water (W) to rock (R) ratios (Taylor, 1971) have been used routinely to estimate the amounts of water involved in fluid-rock interaction in both fossil and active hydrothermal systems. Studies that have developed reactive transport models applied to oxygen isotopes (Baumgartner and Rumble, 1988; Bowman and Willett, 1991; Bowman et al., 1994; Cook et al., 1997; Baumgartner and Valley, 2001) point out that there are several assumptions involved and resulting limitations in applying W/R ratios to isotopically exchanged rocks within hydrothermal systems. In particular, the impact of the prior exchange history of the fluid along flow path(s) to local sites of hydrothermal alteration and isotopic exchange will mean that box model W/R ratios will underestimate actual W/R ratios by an amount that increases

Table 3
Calculated equilibrium $\Delta_{r\text{-}w}$ and $\Delta_{fsp\text{-}w}$, measured $\Delta_{r\text{-}w}$ and $\Delta_{fsp\text{-}w}$, and W/R ratios for well 68-6. W.R. = whole-rock; Eq = equilibrium; FSP = feldspar.

68-6 ID	W.R. $\delta^{18}O$	Eq $\Delta_{r\text{-}w}$ [a]	Measured $\Delta_{r\text{-}w}$ [b]	FSP $\delta^{18}O$	Eq $\Delta_{fsp\text{-}w}$ [a]	Measured $\Delta_{fsp\text{-}w}$ [b]	W/R Closed	W/R Open
996	3.88	9.33	12.55				0.49	0.40
937	4.47	9.33	13.14	6.04	10.17	14.71	0.36	0.31
855	2.55	9.33	11.22				0.80	0.59
789	3.49	9.27	12.16	6.59	10.10	15.26	0.58	0.46
710	5.08	9.27	13.75				0.22	0.20
587	5.78	9.03	14.45				0.06	0.05
556	6.02	8.79	14.69	6.29	9.59	14.96	0.00	0.00
394	3.57	8.04	12.24				0.57	0.45
293	4.07	7.68	12.74				0.45	0.37
208	4.30	7.36	12.97				0.40	0.33
31	4.43	7.36	13.10				0.37	0.31
−60	2.44	6.81	11.11	5.24	7.46	13.91	0.83	0.60
−129	2.87	6.81	11.54				0.73	0.55
−165	1.50	6.81	10.17	4.96	7.46	13.63	1.04	0.71
−230	2.60	6.81	11.27				0.79	0.58
−365	3.78	6.72	12.45	5.64	7.37	14.31	0.52	0.42
−455	4.67	6.51	13.34	6.76	7.13	15.43	0.31	0.27
−581	4.46	6.38	13.13				0.36	0.31
−707	2.94	6.30	11.61				0.71	0.54
−911	2.70	6.06	11.37				0.77	0.57
−1020	0.75	5.94	9.42				1.22	0.80
−1091	0.75	5.88	9.42	3.09	6.46	11.76	1.22	0.80
−1188	0.61	5.79	9.28				1.25	0.81
−1327	0.75	5.50	9.42	3.08	6.05	11.75	1.22	0.80
−1407	2.83	5.60	11.50	3.59	6.16	12.26	0.74	0.55
−1463	0.54	5.77	9.21				1.27	0.82
−1511	0.26	5.98	8.93				1.33	0.85
−1552	−4.60	5.98	4.07	−3.88	6.57	4.79	2.45	1.24
−1594	−1.05	5.73	7.62	1.76	6.30	10.43	1.63	0.97
−1706	0.64	5.00	9.31				1.24	0.81

[a] Equilibrium $\Delta_{r\text{-}w}$ and $\Delta_{fsp\text{-}w}$ fractionation values calculated at pre-production reservoir temperatures using the experimental fractionation factor for An_{50}-water and An_{25}-water (O'Neil and Taylor, 1967), respectively.

[b] Measured $\Delta_{wr\text{-}w}$ and $\Delta_{fsp\text{-}w}$ are the differences between the measured $\delta^{18}O$ values of whole-rock or feldspar, and the measured $\delta^{18}O$ value of the current geothermal fluid (−8.67‰).

with increasing distance along the reactive flow path. The actual amount of fluid involved might have been orders of magnitude higher. As a result, calculated box model W/R ratios should be regarded as minimum estimates of the amounts of fluid involved in hydrothermal alteration and isotopic exchange at specific sites within hydrothermal flow systems. Meteoric waters recharging the Coso geothermal reservoir have experienced considerable $^{18}O/^{16}O$ enrichment, likely resulting from fluid-rock exchange within the deeper, hotter portions of the Coso hydrologic system (Person et al., 2006). However, the geothermal fluids are still well out of oxygen isotope exchange equilibrium with the reservoir host rocks at temperatures from 200 to 350 °C. As a result, these fluids are still chemically (isotopically) reactive, and are capable of producing significant $^{18}O/^{16}O$ depletions in the infiltrated rocks. Consequently, variations in the extent of $^{18}O/^{16}O$ depletion in rocks from local segments of the Coso hydrothermal system—and variations in calculated W/R ratios—will qualitatively reflect variations in fluid fluxes. Hence, the W/R ratios calculated from oxygen isotope ratios are expected to reflect the relative differences in permeability and time-integrated fluid flux for these local segments.

Calculated W/R ratios (atomic oxygen) using both closed and open system box models (Taylor, 1971; Criss and Taylor, 1986) are presented in Tables 3–5. Procedures and data used for these calculations are presented in Appendix B. The $\delta^{18}O$ measurements identify a limited number of localized intervals of much more extensive $^{18}O/^{16}O$ depletion within the Coso reservoir host rocks that have interacted and exchanged isotopically with significantly larger quantities of geothermal fluid (higher calculated W/R ratios). Well 33A-7 has three such intervals of locally more extensive $^{18}O/^{16}O$ depletion and higher calculated W/R ratios at −1170–−1195 msl [$(W/R)_c = 1.94$]; at 413 msl [$(W/R)_c = 1.35$]; and at 1175 msl [$(W/R)_c = 0.71$]. Well 68-6 has one interval at −1552 msl that is characterized by much greater $^{18}O/^{16}O$ depletion and much higher W/R ratio [$(W/R)_c = 2.45$] than elsewhere in the well. In general, calculated W/R ratios for 73-19 are lower than for the other two wells, suggesting that permeability in this well is generally lower than in 68-6 and 33A-7. However, locally higher W/R ratios (closed system) are computed for elevations of −586 (0.57), −565 (0.57), −143 (0.70) and 722 (0.28) meters in well 73-19. The presence of these limited number of discrete intervals of significant $^{18}O/^{16}O$ depletion (and high calculated W/R ratios) in the three wells reflect discrete zones of much higher permeability within low permeability (much less $^{18}O/^{16}O$ depleted) rock. This spatial pattern is consistent with fluid flow that is focused along discrete, higher permeability fracture zones. In all three wells, the elevations of current reservoir fluid production, which are marked by zones of lost circulation and high permeability, correspond to one of these intervals of significant $^{18}O/^{16}O$ depletion—and high W/R ratio (Fig. 7).

Person et al. (2006) inferred the basic structure of the regional groundwater system that could have produced the Coso geothermal system. However, the results of our study show that the $^{18}O/^{16}O$ depletions recorded in the host rocks of the West Flank are poorly correlated with pre-production temperature patterns and better correlated with known intervals of high permeability (e.g. current fluid production zones) (Fig. 6). Further, geochemical and enthalpy data from well tests suggest that the Coso field is divided into a series of hydrologically isolated (fault bounded?), single-phase reservoirs (Williams and McKibben, 1990). These relationships and results suggest that significant permeability structure has been produced within the West flank reservoir by an array of permeable and impermeable fault/fracture

Table 4
Calculated equilibrium $\Delta_{r\text{-}w}$ and $\Delta_{fsp\text{-}w}$, measured $\Delta_{r\text{-}w}$ and $\Delta_{fsp\text{-}w}$, and W/R ratios for well 33A-7. W.R. = whole-rock; Eq = equilibrium; FSP = feldspar.

33A-7 ID	W.R. $\delta^{18}O$	Eq $\Delta_{r\text{-}w}$ [a]	Measured $\Delta_{r\text{-}w}$ [b]	FSP $\delta^{18}O$	Eq $\Delta_{fsp\text{-}w}$ [a]	Measured $\Delta_{fsp\text{-}w}$ [b]	W/R Closed	W/R Open
1251	7.62	23.44	15.11	7.50	25.34	14.99	0.00	0.00
1175	3.7	19.54	11.19				0.71	0.54
1023	5.39	14.03	12.88				0.40	0.34
870	7.45	11.00	14.94				0.03	0.03
718	4.84	11.00	12.33				0.50	0.41
639	5.34	9.78	12.83				0.41	0.35
413	0.2	9.30	7.69				1.35	0.85
261	3.59	8.70	11.08				0.73	0.55
185	3	8.56	10.49	5.49	9.34	12.98	0.84	0.61
−41	4.18	8.20	11.67				0.62	0.49
−283	3.89	7.94	11.38				0.68	0.52
−360	2.71	7.76	10.20				0.89	0.64
−585	1.03	7.39	8.52				1.20	0.79
−689	3.93	7.20	11.42				0.67	0.51
−833	1.6	6.81	9.09				1.09	0.74
−904	−0.44	6.70	7.05				1.46	0.90
−1005	−0.02	6.49	7.47				1.39	0.87
−1005	−1.02	6.49	6.47				1.57	0.94
−1031	−0.98	6.44	6.51				1.56	0.94
−1059	0.14	6.38	7.63				1.36	0.86
−1138	0.51	6.18	8.00	−2.37	6.78	5.12	1.29	0.83
−1170	−2.35	6.06	5.14				1.81	1.03
−1195	−3.08	6.02	4.41	−0.03	6.61	7.46	1.94	1.08
−1230	0.94	6.02	8.43	4.16	6.61	11.65	1.21	0.79
−1276	2.15	5.96	9.64	4.20	6.55	11.69	0.99	0.69
−1284	1.55	5.85	9.04				1.10	0.74
−1314	2.92	5.79	10.41				0.85	0.62
−1343	2.1	5.73	9.59	4.60	6.30	12.09	1.00	0.69
−1402	3.91	5.60	11.40				0.67	0.51
−1487	4.48	5.48	11.97	5.49	6.03	12.98	0.57	0.45
−1603	4.6	5.25	12.09				0.55	0.44
−1632	4.25	5.20	11.74				0.61	0.48
−1661	4.05	5.16	11.54				0.65	0.50
−1690	1.78	5.13	9.27				1.06	0.72
−1721	4.21	5.13	11.70				0.62	0.48
−1751	4.03	5.00	11.52				0.65	0.50
−1782	4.61	4.95	12.10				0.55	0.44
−1812	4.1	4.84	11.59				0.64	0.49
−1873	4.49	4.76	11.98				0.57	0.45
−1934	3.88	4.68	11.37	5.90	5.17	13.39	0.68	0.52

[a] Equilibrium $\Delta_{r\text{-}w}$ and $\Delta_{fsp\text{-}w}$ fractionation values calculated at pre-production reservoir temperatures using the experimental fractionation factor for An_{50}-water and An_{25}-water (O'Neil and Taylor, 1967), respectively.

[b] Measured $\Delta_{wr\text{-}w}$ and $\Delta_{fsp\text{-}w}$ are the differences between the measured $\delta^{18}O$ values of whole-rock or feldspar, and the measured $\delta^{18}O$ value of the current geothermal fluid (−7.49‰).

Table 5
Calculated equilibrium $\Delta_{r\text{-}w}$ and $\Delta_{fsp\text{-}w}$, measured $\Delta_{r\text{-}w}$ and $\Delta_{fsp\text{-}w}$, and W/R ratios for well 73-19. W.R. = whole-rock; Eq = equilibrium; FSP = feldspar.

73-19 ID	W.R. $\delta^{18}O$	Eq $\Delta_{r\text{-}w}$ [a]	Measured $\Delta_{r\text{-}w}$ [b]	FSP $\delta^{18}O$	Eq $\Delta_{fsp\text{-}w}$ [a]	Measured $\Delta_{fsp\text{-}w}$ [b]	W/R Closed	W/R Open
996	6.98	16.10	12.54	7.79	17.43	13.35	0.08	0.08
886	6.61	14.08	12.17				0.13	0.12
877	6.37	14.03	11.93				0.16	0.15
822	7.48	13.35	13.04	8.12	14.47	13.68	0.01	0.01
722	5.52	11.78	11.08				0.28	0.24
490	7.57	8.85	13.13				0.00	0.00
469	6.36	8.62	11.92				0.16	0.15
207	7.16	6.37	12.72				0.06	0.05
195	7.41	6.25	12.97				0.02	0.02
42	6.07	5.47	11.63				0.20	0.18
−49	6.63	5.12	12.19				0.13	0.12
−79	5.91	5.12	11.47				0.22	0.20
−119	4.61	4.92	10.17	6.14	5.42	11.70	0.40	0.33
−143	2.38	5.00	7.94				0.70	0.53
−213	6.3	4.69	11.86	7.26	5.18	12.82	0.17	0.16
−313	5.94	4.55	11.50				0.22	0.20
−395	6.85	4.39	12.41				0.10	0.09
−440	5.13	4.26	10.69				0.33	0.28
−544	5.14	4.63	10.70	6.20	4.69	11.76	0.33	0.28
−565	3.3	4.95	8.86	6.34	4.69	11.90	0.57	0.45
−586	3.3	4.86	8.86				0.57	0.45

[a] Equilibrium $\Delta_{r\text{-}w}$ and $\Delta_{fsp\text{-}w}$ fractionation values calculated at pre-production reservoir temperatures using the experimental fractionation factor for An_{50}-water and An_{25}-water (O'Neil and Taylor, 1967), respectively.

[b] Measured $\Delta_{wr\text{-}w}$ and $\Delta_{fsp\text{-}w}$ are the differences between the measured $\delta^{18}O$ values of whole-rock or feldspar, and the measured $\delta^{18}O$ value of the current geothermal fluid (−5.56‰).

zones. As a result, the flow patterns responsible for the localized $^{18}O/^{16}O$ depletions measured in the West Flank host rocks are likely fracture-controlled and channelized.

Preferential fluid flow within higher permeability fracture zones, with accompanying increase in fluid-rock interaction and $^{18}O/^{16}O$ depletion, is likely a common feature of active hydrothermal systems developed in crystalline rocks. For example, Smith and Suemnicht (1991) measured significantly lower $\delta^{18}O$ values (<−1‰) in what are described as fractured tuffs (well RDO-8) compared to values in less fractured rhyolitic flows and tuffs in other wells at comparable depth in the Long Valley system, consistent with fracture-induced increases in permeability, fluid-rock interaction, and $^{18}O/^{16}O$ depletion within the fractured tuffs. Two clear examples of how fractures and faults define zones of high permeability and control patterns of fluid flow and the extent of $^{18}O/^{16}O$ depletion in fossil hydrothermal systems are the study of the Eocene Sawtooth Ring Zone within the Idaho batholith by Criss and Taylor (1983) and the well-exposed Lake City caldera system, CO by Larson and Taylor (1986b).

4.3. The extent of isotope exchange equilibrium accompanying fluid-rock interaction

Because the pre-production temperatures of the reservoir fluids are known, the equilibrium oxygen isotope fractionations between feldspar and water (equilibrium $\Delta_{fsp\text{-}w}$) can be calculated. These values can be compared to the measured differences in $\delta^{18}O$ between feldspar and the reservoir fluids (measured $\Delta_{fsp\text{-}w}$) (Tables 3–5) to evaluate the extent of exchange equilibrium between the geothermal fluid and feldspar in the reservoir host rocks. If feldspar has incompletely exchanged oxygen isotopes with the low $\delta^{18}O$ geothermal fluid at temperatures below 500 °C, measured $\Delta_{fsp\text{-}w}$ values will be greater than the equilibrium $\Delta_{fsp\text{-}w}$ values. The greater this difference, the farther from exchange equilibrium is the feldspar. The equilibrium fractionation factors are calculated at temperatures measured in the wells prior to production, using the experimental calibration for oxygen isotope fractionation between plagioclase and water from O'Neil and Taylor (1967) and a plagioclase composition of An_{25} (average of measured feldspar compositions in the reservoir rocks; Etzel, 2016).

Fig. 9a depicts the measured $\delta^{18}O$ values of feldspar plotted against the difference between measured $\Delta_{fsp\text{-}w}$ and equilibrium $\Delta_{fsp\text{-}w}$ values. This figure illustrates that the measured $\Delta_{fsp\text{-}w}$ values for most of the sampled intervals are larger than equilibrium $\Delta_{fsp\text{-}w}$ values at measured (pre-production) temperatures and plot to the right of the dashed line (where measured $\Delta_{fsp\text{-}w}$ = equilibrium $\Delta_{fsp\text{-}w}$) in Fig. 9a. This difference indicates that feldspars from most of the sampled intervals in these three wells have not completely exchanged with the geothermal fluid. Two groups of samples with measured $\Delta_{fsp\text{-}w}$ values less than equilibrium $\Delta_{fsp\text{-}w}$ are exceptions. The three feldspar samples with $\delta^{18}O$ values >7.0‰ come from the shallowest, lowest temperature intervals of 33A-7 and 73-19 and have experienced little or no $^{18}O/^{16}O$ depletion relative to their primary $\delta^{18}O$ values. As a result, these feldspars have not experienced any significant interaction with geothermal fluid, and are far from exchange equilibrium with the geothermal fluid (large measured $\Delta_{fsp\text{-}w}$). However given the low temperatures for these three samples, equilibrium $\Delta_{fsp\text{-}w}$ values are even larger. The second exception where measured $\Delta_{fsp\text{-}w}$ values are less than equilibrium $\Delta_{fsp\text{-}w}$ values are the most $^{18}O/^{16}O$ depleted feldspars from 33A-7 and 68-6. These two samples are discussed in the following section.

Fig. 9a also shows that in general, the lower the $\delta^{18}O$ value of the feldspar, the closer the feldspar approaches exchange equilibrium with the geothermal reservoir fluid (e.g., measured $\Delta_{fsp\text{-}w}$ approaches equilibrium $\Delta_{fsp\text{-}w}$). This positive correlation indicates that the feldspar moves progressively toward oxygen isotope exchange equilibrium with the reservoir fluid as the extent of fluid-rock interaction increases (as indicated by progressively greater $^{18}O/^{16}O$ depletion in the feldspar and higher calculated W/R ratio). Experimental studies and theoretical considerations indicate that the rate of oxygen isotope exchange accompanying the types of surface reactions responsible for producing the hydrothermal alteration minerals observed at Coso Hot Springs increases with increasing surface area (Cole and Chakraborty, 2001). The positive correlation between the progressive $^{18}O/^{16}O$ depletion in the feldspar and the increasing approach to oxygen isotopic exchange equilibrium (measured $\Delta_{fsp\text{-}w}$ approaches equilibrium $\Delta_{fsp\text{-}w}$) observed for most of the feldspar samples suggests that increases in permeability of the reservoir host rock produce an increase in surface area of the host rock exposed to geothermal fluid, promoting fluid-rock interaction and isotopic exchange.

Rates of isotopic exchange accompanying hydrothermal alteration also increase dramatically with increasing temperature (Cole and Chakraborty, 2001). However, there is no systematic correlation of temperature with the extent of exchange equilibrium between the feldspar and reservoir fluid within individual wells (Fig. 9b). For feldspar samples from 68 to 6, the excess of measured $\Delta_{fsp\text{-}w}$ compared to equilibrium $\Delta_{fsp\text{-}w}$ value is clearly independent of temperature from 180 °C to 265 °C; for example, across the temperature range of 225–265 °C the difference between the measured $\Delta_{fsp\text{-}w}$ and equilibrium $\Delta_{fsp\text{-}w}$ decreases from 6.3 to −2.0 and then increases to 5.9. A similar situation holds for samples from 33A-7 over the temperature interval from 190 °C to 250 °C; the difference between measured and equilibrium $\Delta_{fsp\text{-}w}$ values changes from 3.6 down to −1.7 and then abruptly increases to 5.

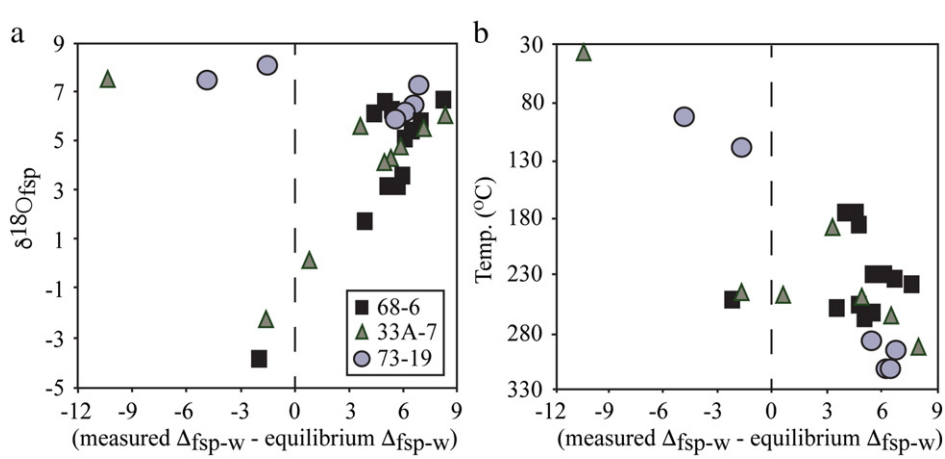

Fig. 9. A) The difference between measured $\Delta_{fsp\text{-}w}$ and equilibrium $\Delta_{fsp\text{-}w}$ plotted against the measured $\delta^{18}O$ value of each feldspar separate. B) The difference between measured $\Delta_{fsp\text{-}w}$ and equilibrium $\Delta_{fsp\text{-}w}$ plotted against measured temperature (pre-production) for the feldspar sample. Equilibrium $\Delta_{fsp\text{-}w}$ is calculated at pre-production temperatures. The dashed line represents equilibrium (measured $\Delta_{fsp\text{-}w}$ = equilibrium $\Delta_{fsp\text{-}w}$) between analyzed feldspar and the pre-production reservoir fluid. Feldspars plotting to right of the dashed line have incompletely exchanged oxygen isotopes with the reservoir fluid.

4.4. Thermal and oxygen isotope evolution of geothermal fluids in the Coso system

Measured $\delta^{18}O$ values of the feldspars are plotted as a function of the pre-production temperature (as measured in the wells) in Fig. 10. Curved lines define the calculated $\delta^{18}O$ values of feldspar in equilibrium with a range of $\delta^{18}O$ values of water, including the pre-production reservoir fluids (solid line). It is apparent that the analyzed feldspars from higher temperatures (>200 °C) in 73-19 plot well above the equilibrium curve for the reservoir fluid, and are far from exchange equilibrium with the reservoir fluid. These feldspars have experienced limited oxygen isotope exchange, either from kinetic barriers to isotopic exchange (from lower temperatures in the past?) or from limited physical contact between the reservoir fluid and rock owing to lower permeability, or both.

Many of the feldspar samples from 68 to 6 and 33A-7 have experienced greater $^{18}O/^{16}O$ depletion and therefore more extensive oxygen isotope exchange, but have not equilibrated with the reservoir fluid (Fig. 10). In contrast, the two feldspars from 33A-7 and 68-6 with the lowest $\delta^{18}O$ values plot below the equilibrium curve for the reservoir fluid. For these two feldspar samples, measured $\Delta_{fsp\text{-}w}$ values are less than equilibrium $\Delta_{fsp\text{-}w}$ values by −1.66 (33A-7_-1138 m) and −1.99 (68-6_-1552) (Fig. 9a). At pre-production temperatures, incomplete isotopic exchange would produce measured $\Delta_{fsp\text{-}w}$ values greater than the equilibrium $\Delta_{fsp\text{-}w}$ values. Therefore, these discrepancies cannot result from incomplete oxygen isotope exchange between the geothermal fluid and the reservoir rocks, because of either slow isotopic exchange kinetics or lack of physical contact between fluid and feldspar crystals. Measured $\Delta_{fsp\text{-}w}$ less than equilibrium $\Delta_{fsp\text{-}w}$ requires that the isotopic exchange took place either at higher temperatures and/or with a reservoir fluid of lower $\delta^{18}O$ value. Fig. 10 shows that temperatures would need to increase by 55 °C (to 307 °C) and 42 °C (to 288 °C) in 68-6 and 33A-7, respectively, for the most $^{18}O/^{16}O$-depleted feldspars from each well to be in exchange equilibrium with the reservoir fluid. Alternatively, the $\delta^{18}O$ values of geothermal fluids would need to decrease by 1.98‰ and 1.66‰ in 68-6 and 33A-7, respectively (Tables 3, 4; Fig. 10). A lower $\delta^{18}O$ value of the reservoir fluid in the past implies a decrease in the initial $\delta^{18}O$ value of the meteoric water source, and/or an increase in the W/R ratio (and permeability) for these sections of geothermal system.

Oxygen isotope disequilibrium between $^{18}O/^{16}O$ depleted rocks and current reservoir fluids at present temperatures has been noted in other active hydrothermal systems as well. Sturchio et al. (1990) documented oxygen isotope disequilibrium between many of their samples of silica minerals from fractures and vugs in drill core from Yellowstone with present-day thermal waters at current temperatures. They attributed this disequilibrium to $^{18}O/^{16}O$ enrichment of thermal fluids from the transient effects of decompressional boiling and/or increased fluid-

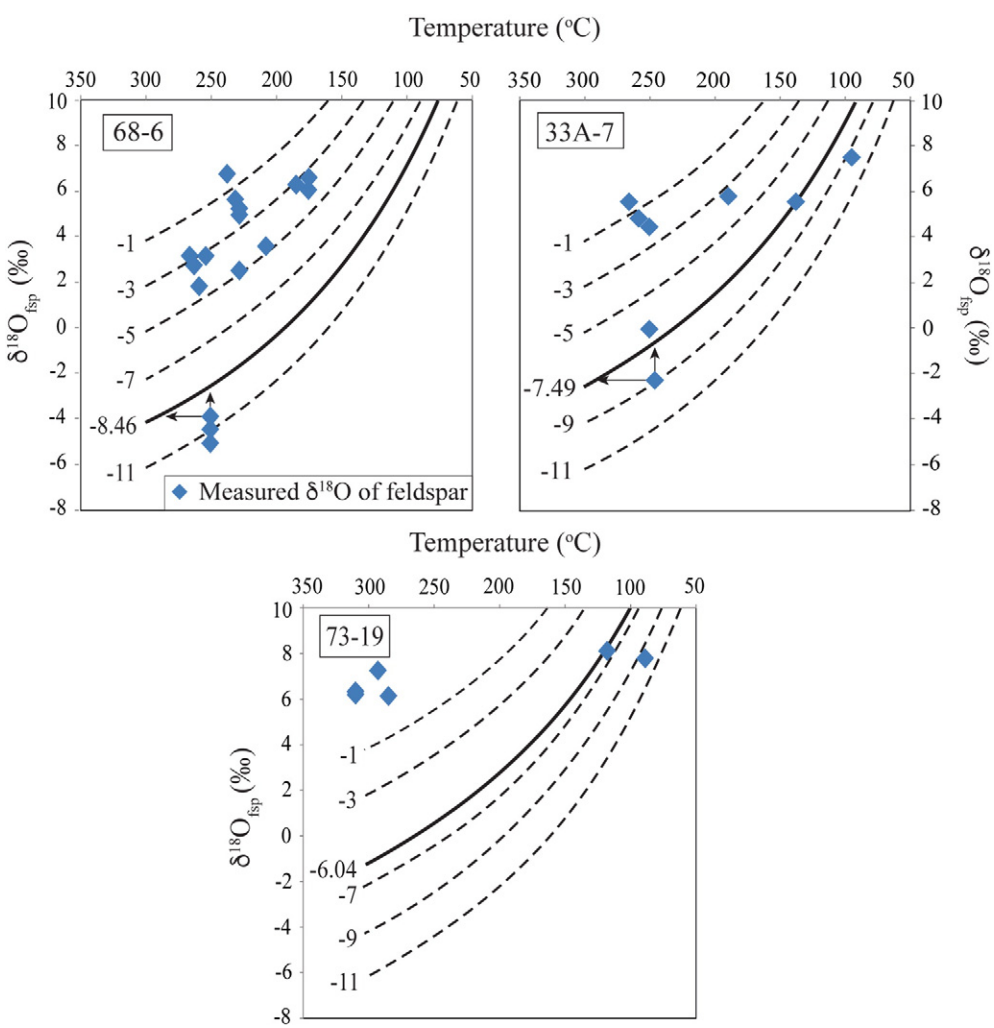

Fig. 10. Measured $\delta^{18}O$ values of feldspars plotted as a function of pre-production temperatures (as measured in the wells). Curved lines define the calculated $\delta^{18}O$ values of feldspar in exchange equilibrium with a range of $\delta^{18}O$ values of water (values specified next to each curve), including the pre-production reservoir fluids in these wells (solid line), as a function of temperature. Arrows indicate changes in temperature or $\delta^{18}O$ of reservoir fluid needed for the most ^{18}O-depleted feldspar in 68-6 and 33A-7 to achieve oxygen isotope exchange equilibrium with the geothermal reservoir fluids.

rock interaction/exchange in newly-formed fractures. Smith and Suemnicht (1991) attributed discrepancies between measured and calculated $\delta^{18}O$ values of host rocks in parts of the Long Valley system to record fluid-rock interaction (and oxygen isotope exchange) at higher temperatures in the past. These discrepancies noted for Yellowstone, Long Valley and Coso reflect the transient nature of the thermal and fluid-rock interaction regimes in active hydrothermal systems.

5. Conclusions

The patterns and extent of $^{18}O/^{16}O$ depletions measured in the reservoir rocks of the Coso Hot Springs geothermal system, combined with clay mineral alteration patterns, record significantly varying degrees of fluid-rock interactions. These patterns provide insights into the role of fracture-controlled permeability in this geothermal system. Our results indicate the following:

- Clay mineral distribution in three wells along the West Flank is not always closely correlated with the distribution expected from preproduction temperatures measured in these wells. There is, however, a general correlation between greater and more widespread $^{18}O/^{16}O$ depletion in the northern part of the West Flank with a thinner smectite zone and disappearance of the illite/smectite zone. This correlation suggests that clay mineral distributions in the Coso Hot Springs field is a function of both the extent of fluid-rock interaction and temperature.
- Whole-rock and feldspar $\delta^{18}O$ analyses define patterns of $^{18}O/^{16}O$ depletion in the West Flank distinct from those expected from regional metamorphism. These oxygen isotope analyses show that the reservoir rocks have experienced a wide range of $^{18}O/^{16}O$ depletion, from negligible depletion below primary $\delta^{18}O$ values of +7.5‰ to $\delta^{18}O$ values as low as −6‰ for feldspar. This large range indicates that the reservoir rocks have experienced significant variation in the extent of fluid-rock interaction.
- Detailed $\delta^{18}O$ measurements of whole rock and feldspar samples from three wells along the West Flank identify a limited number of localized intervals of extensive $^{18}O/^{16}O$ depletion where the host rocks have interacted and exchanged isotopically with significant quantities of geothermal fluid (high calculated W/R ratios). The local zones of maximum $^{18}O/^{16}O$ depletion in each well correspond closely with the depths of the current production zones (intervals of high permeability). Rocks between these intervals have experienced much less exchange. These patterns likely reflect that permeability in the reservoir host rock is fracture-controlled.
- Most analyzed feldspars have $\delta^{18}O$ values too high to have completely exchanged with the reservoir fluid. The analyses also show that in general, the lower the $\delta^{18}O$ value of the feldspar (the greater the extent of fluid-rock interaction), the closer the feldspar approaches isotope exchange equilibrium with the geothermal fluid. This positive correlation suggests that fracture-induced increases in permeability of the reservoir host rock increase mineral/grain surface area exposed to geothermal fluids, promoting fluid-rock interaction and isotopic exchange.
- There is no systematic correlation of temperature with either the extent of $^{18}O/^{16}O$ depletion or the extent of exchange equilibrium between the feldspar and reservoir fluid in the West Flank. This is particularly the case for 73-19, where rock host has experienced only moderate and highly localized $^{18}O/^{16}O$ depletion despite having the highest measured temperatures in the three wells. Thus in the West Flank at Coso Hot Springs (a crystalline-rock-hosted geothermal system), permeability is as, or more important than temperature in driving fluid-rock interaction and isotopic exchange.
- The three feldspar samples with the lowest $\delta^{18}O$ values are all from current production zones in the reservoir. These feldspars are highly depleted in $^{18}O/^{16}O$ and therefore have experienced extensive fluid-rock interaction and isotopic exchange. However, two of these feldspar separates have measured $\Delta_{fsp\text{-}w}$ < equilibrium $\Delta_{fsp\text{-}w}$ which requires that they have equilibrated with the pre-production reservoir fluid at higher temperature, or with a lower $\delta^{18}O$ reservoir fluid. These discrepancies suggest that the West Flank of the Coso geothermal system was hotter and/or characterized by higher permeability (higher W/R ratio) during fluid-rock exchange in the past.
- The results of this study corroborate those of a number of previous oxygen isotope studies of (mostly) fossil hydrothermal systems, in documenting the connection between the extent of $^{18}O/^{16}O$ depletion, the extent of fluid-rock interaction and permeability in crystalline rock hosts to hydrothermal systems. These connections suggest that mapping patterns of $^{18}O/^{16}O$ depletion can be another exploration tool to define permeability structure, identify higher permeability zones, and constrain fluid flow patterns – past and present – in active hydrothermal systems, and to help facilitate development of enhanced geothermal systems.

Acknowledgements

U.S. Department of Energy (DOE) grant (DE-EE0005521) to Moore is gratefully acknowledged. Terra-Gen has provided access to well cuttings, and a variety of geological, geochemical and geophysical data on the Coso Hot Springs geothermal system. We thank Shaul Hurwitz and one other anonymous reviewer for their thoughtful and constructive comments that helped enhance the overall quality of this paper. We thank Clay Jones for his assistance with XRD analyses.

Appendix A. Supplementary data

Supplementary data to this article can be found online at http://dx.doi.org/10.1016/j.jvolgeores.2016.11.014.

References

Adams, M.C., Moore, J.N., Bjornstad, S., Norman, D.I., 2000. Geologic history of the Coso geothermal system. Trans. Geotherm. Res. Counc. 24, 205–209.
Bartley, J.M., Glazner, A.F., Coleman, D.S., Kylander-Clark, A., Mapes, R., Friedrich, A.M., 2007. Large Laramide dextral offset across Owens Valley, California, and its possible relation to tectonic unroofing of the southern Sierra Nevada. Geol. Soc. Am. Spec. Pap. 434, 129–148.
Baumgartner, L.P., Rumble III, D., 1988. Transport of stable isotopes-I. Development of continuum theory for stable isotope transport. Contrib. Mineral. Petrol. 98, 417–430.
Baumgartner, L.P., Valley, J.W., 2001. Stable isotope transport and contact metamorphic fluid flow. In: Valley, J.W., Cole, D.R. (Eds.), Stable Isotope Geochemistry. Reviews in Mineralogy and Geochemistry 43, pp. 415–461.
Bigeleisen, J., Perlman, M.L., Prosser, H.C., 1952. Conversion of hydrogenic materials for isotopic analysis. Anal. Chem. 24, 1356–1357.
Bishop, B., Bird, D., 1987. Variation in sericite compositions from fracture zones within the Coso Hot Springs geothermal system. Geochim. Cosmochim. Acta 51, 1245–1256.
Bowman, J.R., Willett, S.D., 1991. Spatial patterns of oxygen isotope exchange during one-dimensional fluid infiltration. Geophys. Res. Lett. 18, 971–974.
Bowman, J.R., Willett, S.D., Cook, S.J., 1994. Oxygen isotopic transport and exchange during fluid flow: one-dimensional models and applications. Am. J. Sci. 294, 1–55.
Browne, P., 1978. Hydrothermal alteration in active geothermal fields: a geochemical review. Annu. Rev. Earth Planet. Sci. 6, 229–250.
Browne, P., 1984. Lectures on geothermal geology and petrology: UNU Geothermal Training Programme, Iceland. Report 1984-2.
Clayton, R.N., Mayeda, T.K., 1963. The use of bromine pentafluoride in the extraction of oxygen from oxides and silicates for isotopic analysis. Geochim. Cosmochim. Acta 27, 43–52.
Cole, D.R., Chakraborty, S., 2001. Rates and mechanisms of isotopic exchange. In: Valley, J.W., Cole, D.R. (Eds.), Stable Isotope Geochemistry. Reviews in Mineralogy and Geochemistry 43, pp. 83–223.
Cole, D.R., Ohmoto, H., Jacobs, G.K., 1992. Isotopic exchange in mineral-fluid systems: III. Rates and mechanisms of oxygen isotope exchange in the system granite-H_2O ± NaCl ± KCl at hydrothermal conditions. Geochim. Cosmochim. Acta 56, 445–466.
Cook, S.J., Bowman, J.R., Forster, C.B., 1997. Contact metamorphism surrounding the Alta Stock: Finite element model simulation of heat- and $^{18}O/^{16}O$ mass-transport during prograde metamorphism. Am. J. Sci. 297, 1–55.
Criss, R.E., Taylor Jr., H.P., 1983. An $^{18}O/^{16}O$ and D/H study of Tertiary hydrothermal system in the southern half of the Idaho batholith. GSA Bull. 94, 640–663.
Criss, R.E., Taylor Jr., H.P., 1986. Meteoric-hydrothermal systems. In: Valley, J.W., Taylor Jr., H.P., O'Neil, J.R. (Eds.), Stable Isotopes in High Temperature Geological Processes. Reviews in Mineralogy 16, pp. 373–422.

Davatzes, N.C., Hickman, S.H., 2010. The feedback between stress, faulting, and fluid flow: lessons from the Coso geothermal field, USA: Proceedings world geothermal congress 2010, Bali, Indonesia. pp. 1–14.
Duffield, W.A., Bacon, C.R., Dalrymple, G.B., 1980. Late Cenozoic volcanism, geochronology, and structure of the Coso Range, Inyo County, California. J. Geophys. Res. 85, 2381–2404.
Epstein, S., Mayeda, T.K., 1953. Variations of O^{18} content of waters from natural sources. Geochim. Cosmochim. Acta 4, 213–224.
Etzel, T.M., 2016. Oxygen Isotope Composition and Tourmaline Mineral Chemistry of the Coso and Darajat Geothermal Systems. Masters thesis. University of Utah.
Faure, K., Matsuhisa, Y., Metsugi, H., Mizota, C., Hayashi, S., 2002. The Hishikari Au-Ag epithermal deposit, Japan: oxygen and hydrogen isotope evidence in determining the source of paleohydrothermal fluids. Econ. Geol. 97, 481–498.
Forester, R.W., Taylor Jr., H.P., 1980. Oxygen, hydrogen, and carbon isotope studies of the Stony Mountain Complex, western San Juan Mountains, Colorado. Econ. Geol. 75, 362–383.
Fournier, R.O., Thompson, J.M., Austin, C.F., 1980. Interpretation of chemical analyses of waters collected from two geothermal wells at Coso, California. J. Geophys. Res. 85, 2405–2410.
Haas, J.L., 1971. The effect of salinity on the maximum thermal gradient of a hydrothermal system at hydrostatic pressure. Econ. Geol. 31, 167–171.
Henley, R.W., Ellis, A.J., 1983. Geothermal systems ancient and modern: a geochemical review. Earth-Sci. Rev. 19, 1–50.
Hulen, J.B., 1978. Geology and alteration of the Coso Geothermal Area, Inyo County, California: University of Utah Research Institute Report DOE/ID/28392-4. pp. 1–28.
Kaven, J.O., Hickman, S.H., Davatzes, N.C., 2012. Using micro-seismicity and seismic velocities to map subsurface geologic and hydrologic structure within the Coso geothermal field, California: Proceedings, 37th workshop on Geothermal Reservoir Engineering, Stanford, CA. pp. 1085–1092.
Kovac, K.M., Moore, J., McCulloch, D.E., 2004. Geology and mineral paragenesis study within the Coso-EGS project: Proceedings, 29th workshop on Geothermal Reservoir Engineering, Stanford, CA. pp. 262–267.
Kovac, K.M., Moore, J.N., Lutz, S.J., 2005. Geologic Framework of the East Flank, Coso Geothermal Field: Implications for EGS Development: Proceedings, 30th Workshop on Geothermal Reservoir Engineering. pp. 486–492.
Kurliovitch, L., Norman, D., Heizler, M., Moore, J., McCulloch, J., 2003. $^{40}Ar/^{39}Ar$ Thermal History of the Coso Geothermal Field: Proceedings, 28th Workshop on Geothermal Reservoir Engineering. CA, Stanford, pp. 110–116.
Lackey, J.S., Valley, J.W., Chen, J.H., Stockli, D.F., 2008. Dynamic magma systems, crustal recycling, and alteration in the central Sierra Nevada Batholith: the oxygen isotope record. J. Petrol. 49, 1397–1426.
Lambert, S.J., Epstein, S., 1980. Stable isotope investigations of an active geothermal system in Valles Caldera, Jemez Mountains, New Mexico. J. Volcanol. Geotherm. Res. 8, 111–129.
Larson, P.B., Taylor Jr., H.P., 1986a. An oxygen-isotope study of water-rock interaction in the granite of Cataract Gulch, western San Juan Mountains. GSA Bull. 97, 505–515.
Larson, P.B., Taylor Jr., H.P., 1986b. An oxygen isotope study of hydrothermal alteration in the Lake City Caldera, San Juan Mountains, Colorado. J. Volcanol. Geotherm. Res. 30, 47–82.
Lutz, S.J., Moore, J.N., 1997. Petrographic and X-ray diffraction study of 130 cuttings samples from six wells in the Coso geothermal area, California, unpublished CalEnergy Corporation Report.
Lutz, S.J., Moore, J.N., Copp, J.F., 1996. Integrated mineralogical and fluid inclusion study of the Coso geothermal system, California: Proceedings, 21st workshop on geothermal reservoir engineering, Stanford, CA. pp. 187–194.
Manley, C.R., Bacon, C.R., 2000. Rhyolite thermobarometry and the shallowing of the Magma Reservoir, Coso Volcanic Field, California. J. Petrol. 41, 149–174.
Masi, U., O'Neil, J.R., Kistler, R.W., 1981. Stable isotope systematics in Mesozoic granites of central and northern California and southwestern Oregon. Contrib. Mineral. Petrol. 76, 116–126.
Mauk, J.L., Simpson, M.P., 2007. Geochemistry and stable isotope composition of altered rocks at the Golden Cross epithermal Au-Ag deposit, New Zealand. Econ. Geol. 102, 841–871.
McConnell, V.S., Valley, J.W., Eichelberger, J.C., 1997. Oxygen isotope compositions of intracaldera rocks: hydrothermal history of the Long Valley Caldera, California. J. Volcanol. Geotherm. Res. 76, 83–109.
Monastero, F.C., Katzenstein, A.M., Miller, J.S., Unruh, J.R., Adams, M.C., Richards-Dinger, K., 2005. The Coso geothermal field: a nascent metamorphic core complex. Geol. Soc. Am. Bull. 117, 1534–1553.
Moore, J.N., Gunderson, R.P., 1995. Fluid inclusion and isotopic systematics of an evolving magmatic-hydrothermal system. Geochim. Cosmochim. Acta 59, 3887.
Moore, D.M., Reynolds, R.C., 1997. X-ray Diffraction and the Identification and Analysis of Clay Minerals. Oxford University Press, New York, New York 378 p.
Moore, J.N., Adams, M.C., Bishop-Gollan, B., Copp, J.F., Hirtz, P., 1990. In: Moore, J.L., Erskine, M. (Eds.), Geochemical structure of the Coso geothermal System, California: American Association of Petroleum Geologists Guidebook, Coso Field Trip, AAPG EMD #1, pp. 25–39.
O'Neil, J.R., Taylor Jr., H.P., 1967. The oxygen isotope and cation exchange chemistry of feldspars. Am. Mineral. 52, 1414–1437.
Person, M.A., Sabin, A.E., Unruh, J.R., Gable, C.W., Zyvoloski, G.A., Monastero, F.C., 2006. Isotope transport and exchange within the Coso geothermal system. Proceedings, 30th Workshop on Geothermal Reservoir Engineering. 30, pp. 159–164.
Pope, E.C., Bird, D.K., Arnorsson, S., Giroud, N., 2016. Hydrogeology of the Krafla geothermal system, northeast Iceland. Geofluids 16, 175–197.
Reasenberg, P., Ellsworth, W., Walter, A., 1980. Teleseismic evidence for a low-velocity body under the Coso Geothermal Field. J. Geophys. Res. 85, 2471–2483.
Reyes, A.G., 1990. Petrology of Philippines geothermal systems and the application of alteration mineralogy to their assessment. J. Volcanol. Geotherm. Res. 43, 279–309.
Smith, B.M., Suemnicht, G.A., 1991. Oxygen isotope evidence for past and present hydrothermal regimes of Long Valley caldera, California. J. Volcanol. Geotherm. Res. 48, 319–339.
Spicuzza, M.J., Valley, J.W., McConnell, V.S., 1998. Oxygen Isotope Analysis of Whole Rock Via Laser Fluorination: An Air-lock Approach: GSA Abstracts With Programs. 30 p. 80.
Steiner, A., 1968. Clay minerals in hydrothermally altered rocks in Wairakei, New Zealand. Clay Clay Miner. 16, 193–213.
Sturchio, N.C., Keith, T.E.C., Muehlenbachs, K., 1990. Oxygen and carbon isotope ratios of hydrothermal minerals from Yellowstone drill cores. J. Volcanol. Geotherm. Res. 40, 23–37.
Taylor Jr., H.P., 1971. Oxygen isotope evidence for large-scale interaction between meteoric ground waters and Tertiary granodiorite intrusion, western Cascade Range, Oregon. J. Geophys. Res. 76, 7855–7874.
Taylor Jr., H.P., 1973. $^{18}O/^{16}O$ evidence for meteoric-hydrothermal alteration and ore deposition in the Tonopah, Comstock Lode, and Goldfield Mining districts Nevada. Econ. Geol. 68, 747–764.
Taylor Jr., H.P., 1974. The application of oxygen and hydrogen isotopes studies to problems of hydrothermal alteration and ore deposition. Econ. Geol. 69, 843–883.
Taylor Jr., H.P., Forester, R.W., 1979. An oxygen and hydrogen isotope study of the Skaergaard intrusion and its country rocks: a description of a 55-M.Y. old fossil hydrothermal system. J. Petrol. 20, 355–419.
Truesdell, A.H., 1984. Stable isotopes in hydrothermal systems in fluid-mineral Equilibria in Hydrothermal Systems. In: Robertson, J.M. (Ed.), Reviews in Economic Geology. 1, pp. 129–141.
Valley, J.W., Graham, C.M., 1996. Ion microprobe analysis of oxygen isotope ratios in quartz from Skye granite: healed micro-cracks, fluid flow, and hydro-thermal exchange. Contrib. Mineral. Petrol. 124 (3/4), 225–234.
Valley, J.W., Kita, N.T., 2009. *In situ* oxygen isotope geochemistry by ion microprobe. MAC Short Course. In: Fayek, M. (Ed.), Secondary Ion Mass Spectrometry in the Earth Sciences. 41, pp. 19–63.
Valley, J.W., Kitchen, N., Kohn, M.J., Niendorf, C.R., Spicuzza, M.J., 1995. UWG-2, A garnet standard for oxygen isotope ratio-Strategies for high precision and accuracy with laser heating. Geochim. Cosmochim. Acta 59, 5223–5231.
White, A.F., Peterson, M.L., 1991. Chemical equilibrium and mass balance relationships associated with the Long Valley hydrothermal system, California, U.S.A. J. Volcanol. Geotherm. Res. 48, 283–302.
Williams, A.E., McKibben, M.A., 1990. Isotopic and chemical constraints on reservoir fluids from the Coso geothermal field, California. Proceedings, 14th Workshop on Geothermal Reservoir Engineering, Stanford, CA, pp. 1545–1552.
Wilson, C.K., Jones, C.H., Gilbert, H.J., 2003. A single-chamber silicic magma system inferred from shear-wave discontinuities of the crust and uppermost mantle, Coso geothermal area, California. J. Geophys. Res. 108, B5.